Tuuli Nissinen

OPTICS MEASUREMENTS WITH THE TRANSVERSE DAMPER IN THE LARGE HADRON COLLIDER

CERN-THESIS-2024-245
16/09/2024

Master's Thesis
Faculty of Engineering and Natural Sciences
Examiners: Dr. Félix Carlier
Prof. Esa Räsänen
September 2024

ABSTRACT

Tuuli Nissinen: Optics Measurements with the Transverse Damper in the Large Hadron Collider
Master's Thesis
Tampere University
Master's Programme in Science and Engineering
September 2024

Effective control of beam optics is critical for achieving the luminosity targets in particle colliders such as the Large Hadron Collider (LHC). The search of new discoveries requires even higher beam intensities and smaller beam sizes at collision points, emphasizing the significance of optics corrections.

Current optics measurement techniques in the LHC are limited to restricted machine conditions and low-intensity bunches using the ac dipole. Until now, these methods have provided the required precision for sufficient luminosity production. However, with increasing beam intensities, possible deviations in optics quality are introduced that need to be identified and corrected accordingly.

The LHC Transverse Damper (ADT) used in ac dipole -like mode offers an alternative by providing a coherent transverse beam excitation with a low oscillation amplitude, even with operational beams. As the oscillation amplitude of the ADT is low, improvements in spectral resolution are necessary to obtain a comparable measurement quality to the ac dipole. These improvements could be achieved through upgrades, such as increasing the number of acquired turns, increasing the oscillation amplitude and decreasing the tune split.

This thesis presents the advancements made in optics measurements with the ADT in the LHC using pilot bunches. Enhancements in the spectral resolution were achieved by increasing the number of acquired turns and the oscillation amplitude. Between ADT and ac dipole excitations, linear optics showed a good agreement at injection energy, validating the usage of ADT for optics measurements with low-intensity bunches.

Furthermore, secondary spectral lines arising from nonlinear contributions were observed with the ADT. The analysis of the normal sextupolar terms show promising results for low-amplitude nonlinear optics measurements in the future. Finally, some observed limitations of the ADT are discussed and their effect on the ADT performance is considered.

The presented results offer a clear path towards performing optics measurements in operational conditions in the LHC, marking a significant step forward in operation of the particle collider.

Keywords: ADT, transverse damper, optics, accelerator, LHC, CERN

The originality of this thesis has been checked using the Turnitin OriginalityCheck service.

TIIVISTELMÄ

Tuuli Nissinen: Optiikan mittaaminen poikittaisvaimentimella Large Hadron Colliderissa
Diplomityö
Tampereen yliopisto
Teknis-luonnontieteellinen DI-ohjelma
Syyskuu 2024

Hiukkassuihkuoptiikan hyvä hallinta on ratkaisevan tärkeää hiukkastörmäyttimien, kuten Large Hadron Collider (LHC) -törmäyttimen luminositeettitavoitteiden saavuttamiseksi. Uusien löytöjen mahdollistamiseksi vaaditaan entistä suurempia hiukkassuihkun intensiteettejä sekä pienempiä sädekokoja törmäyspisteissä, jolloin optiikan korjausten merkitys korostuu entisestään.

LHC:n nykyisiä optiikan mittaustekniikoita voidaan käyttää vain rajoitetuissa laiteolosuhteissa ja matalaintensiteettisillä hiukkassuihkuilla hyödyntäen ac-dipolia. Tähän mennessä nämä metodit ovat tarjonneet riittävän tarkkuuden tarvittavan luminositeettituotannon saavuttamiseksi. Hiukkassuihkujen intensiteettien kasvaessa mahdolliset poikkeamat optiikan laadussa täytyy ottaa huomioon ja korjata tarpeen mukaan.

LHC:n poikittaisvaimenninta (ADT, eng. Transverse Damper) voidaan käyttää ac-dipolin kaltaisesti tuottamaan koherentti poikittainen viritys hiukkassuihkulle. Virityksen amplitudi on matala, joten sitä on turvallista käyttää myös korkeaintensiteettisiin hiukkassuihkuihin. Koska ADT:n oskillaatioamplitudi on pieni, spektriresoluutiota on parannettava, jotta mittausten laatu olisi verrattavissa ac-dipoliin. Resoluutiota voidaan parantaa erilaisilla toimenpiteillä, kuten lisäämällä tallennettujen kierrosten lukumäärää, kasvattamalla oskillaatioamplitudia ja pienentämällä vire-erotusta.

Tässä diplomityössä esitellään ADT:llä tehdyt optiikan mittaukset käyttäen pilottikimppuja. Taajuusspektrin resoluutiota parannettiin lisäämällä tallennettujen kierrosten määrää sekä kasvattamalla oskillaatioamplitudia. ADT:n ja ac-dipolin välillä lineaarinen optiikka osoitti hyvää yhdenmukaisuutta injektioenergiassa osoittaen ADT:n soveltuvuuden optiikan mittaamiseen matalan intensiteetin hiukkassuihkujen kanssa.

Lisäksi ADT:llä havaittiin epälineaarisista kontribuutioista johtuvia sekundaarisia spektriviivoja taajuusspektrissä. Normaalien sekstupolitermien analyysi osoittaa lupaavia tuloksia epälineaarisen optiikan mittaamiseen matala-amplitudisella hiukkassuihkulla tulevaisuudessa. Lopuksi käsitellään joitakin ADT:n havaittuja rajoitteita sekä niiden vaikutusta ADT:n suorituskykyyn.

Esitetyt tulokset tarjoavat selkeän tien kohti optiikan mittaamista operatiivisissa olosuhteissa LHC:ssä, mikä on merkittävä edistysaskel törmäyttimen operoinnissa.

Avainsanat: ADT, poikittaisvaimennin, optiikka, kiihdytin, LHC, CERN

Tämän julkaisun alkuperäisyys on tarkastettu Turnitin OriginalityCheck -ohjelmalla.

PREFACE

The research conducted in this thesis has been performed in the Optics Measurements and Corrections (OMC) -team at CERN.

First, I would like to thank my CERN supervisor, Félix Carlier, for sharing your extensive knowledge on beam dynamics with me. I am extremely grateful to you for helping me throughout the incredible journey I had while at CERN and afterwards. I also want to thank my university supervisor, Esa Räsänen, for providing valuable feedback on the thesis.

Working at CERN as a technical student not only gave me heaps of new academic knowledge, but also confidence on my work and myself. Spending nights at the CERN Control Centre doing measurements with the OMC-team, presenting my first article at a conference and attending the CERN Accelerator School in sunny Spain are just some of the highlights I encountered during the year and will never forget. A sincere thank you goes to all the wonderful colleagues I met during my stay.

Lastly, I want to express my gratitude to friends and family in Finland and abroad for providing unforgettable memories throughout these past years. Thank you and kiitos!

Tampere, 17th September 2024

Tuuli Nissinen

CONTENTS

1. INTRODUCTION

Measurement and correction of optics functions in particle colliders have a direct effect on the luminosity reach and the operability of the machine. Current and future projects at the intensity frontier of accelerator research aim to increase the luminosity in order to gather more data and discover new phenomena. The High-Luminosity upgrade of the Large Hadron Collider (LHC) aims to increase the total integrated luminosity by a factor of 10 compared to current values. Achieving this requires reducing the beam size at the collision points while simultaneously increasing the bunch intensity [1].

As the beam intensities increase and optics are pushed to more challenging regimes, measuring and correcting optics in the machine is becoming even more crucial. Optics challenges arise from the interplay of optics and collective effects such as beam-beam interactions and electron clouds [2–6], emphasizing the need for a deeper understanding of the optics in operational conditions.

The preferred method to measure optics in the LHC has been beam-based turn-by-turn optics measurements from beam excitations with the ac dipole [7–9]. It offers fast, accurate and repeatable measurements. Through transverse excitations from the ac dipole, the β-beating is accurately measured and corrected to a level of a few percent [10]. Additionally, extensive research of measuring and correcting nonlinear errors relies on ac dipole measurements [11, 12].

For machine protection purposes, the ac dipole can only be used with low intensity beams. Until now, this has been enough to measure and correct the optics with pilot bunches. With full operational beam intensities, deviations in the optics compared to lower intensities are estimated to be within tolerances, but further validation is needed for confirmation.

The LHC Transverse Damper (ADT) [13] can be operated in ac dipole -like mode to provide a transverse excitation to the beam. Due to its weaker strength, the ADT is considered safe for use with operational beams, and therefore allows to extend the preferred optics measurement technique to new machine states.

This thesis presents the first optics measurements taken in the LHC with the ADT. Chapter 2 introduces the LHC and its operation during Run 3. The theoretical background of transverse beam dynamics concepts relevant to this thesis is given in Chapter 3. A typical process of optics measurements in the LHC is discussed in Chapter 4, and Chapter

5 presents the analysis of optics measurements with the ADT taken in 2023. Lastly, Chapter 6 summarizes the project and provides outlook on future studies. Appendix A presents the paper including part of the results analysed for this thesis, presented at the 68th ICFA Advanced Beam Dynamics Workshop on High-Intensity and High-Brightness Hadron Beams (HB2023).

2. LARGE HADRON COLLIDER

The Large Hadron Collider (LHC) [14] is a 27-kilometre two-ring hadron accelerator located at the European Organization for Nuclear Research (CERN, *Conseil Européen pour la Recherche Nucléaire* in French) near Geneva, Switzerland. It is currently the largest and most powerful hadron collider in the world with an energy of up to 6.8 TeV per beam for proton-proton collisions that are provided to four particle detectors; ATLAS [15], CMS [16], LHCb [17], and ALICE [18]. The LHC led to the discovery of the Higgs boson by ATLAS and CMS in 2012 [19, 20], which completed the Standard Model [21]. Current research aims to further constraint the Standard Model, as well as look beyond it. Some current research topics include the imbalance of matter and antimatter and the existence of dark matter and dark energy.

In order to accelerate particles to energies needed for high-energy physics research, particles pass through several accelerators referred to as the injector chain before reaching the LHC. The path of the particles throughout the chain is illustrated in Fig. 2.1 together with a multitude of other experiments at CERN. Protons are first accelerated to an energy of 160 MeV in LINAC4 [22] before being injected into the Proton Synchrotron Booster (PSB) [23] and accelerated to 2 GeV. Next, the particles are extracted into the Proton Synchrotron (PS) [24] and accelerated to 26 GeV to be injected into the Super Proton Synchrotron (SPS) [25] with further acceleration to 450 GeV. Eventually, the particles make their way to the LHC with the injection energy of 450 GeV. In addition to protons, physics research is conducted in the LHC using heavy ions, such as lead. Lead ions are injected from LINAC3 [26] to LEIR [27] and then onwards to the PS, following the same accelerator chain as with protons until reaching the LHC.

Particles collide in the LHC in four interaction points (IPs), each one equipped with a high-precision detector. The two main detectors, ATLAS (A Toroidal LHC ApparatuS) and CMS (Compact Muon Solenoid) are general-purpose detectors to study a broad variety of particle physics. ALICE (A Large Ion Collider Experiment) studies the formation of quark-gluon plasma in lead ion collisions. The fourth detector, LHCb (Large Hadron Collider beauty experiment), is dedicated for investigating symmetries between matter and antimatter.

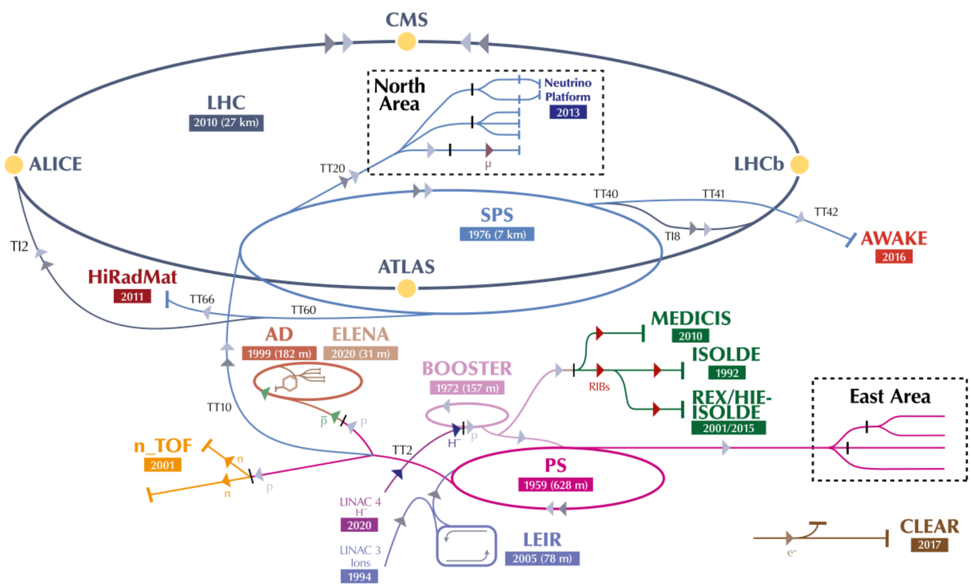

Figure 2.1. *Illustration of the CERN accelerator complex in 2022. Adapted from [28].*

The measurement cycle of the LHC starts with ramping the magnets to the injection energy of 450 GeV before injecting a single, low-intensity bunch called a pilot or probe into the machine from the SPS. This pilot bunch is injected for machine protection reasons in order to prevent damaging the machine components before injecting bunches with a higher intensity [29]. With beam presence, bunches of higher intensity can be injected using a specified filling scheme determining the number of bunches and bunch spacing. After the machine is full, the beams are accelerated to collision energy (6.8 TeV in 2023) using radio frequency (RF) cavities, and simultaneously the magnet fields are ramped up. Before colliding the two beams, the beam size at the IPs is reduced in order to get the most collisions. Finally, separation bumps are collapsed, allowing for collisions and data collection from the experiments. Once the beam intensity is too low for adequate luminosity production, the beams are safely dumped and magnets are ramped down. After this, the cycle is repeated.

In order to have the machine in the most optimal conditions for collisions and luminosity production, a thorough commissioning campaign [30] is organised. After a longer shutdown period, for example the year-end technical shutdown, the hardware is first commissioned without beam. Before injecting the beam into the machine, a machine checkout period is performed where all the systems are validated and a dry run through the measurement cycle is performed. Afterwards, commissioning with beam is the final stage to prepare for the luminosity production. Beam commissioning is a time-intensive period for correcting and optimising the machine, since major changes are not made during physics production.

3. ACCELERATOR AND BEAM PHYSICS

This chapter introduces the theoretical background of topics of accelerator and beam physics relevant for this thesis. The topics are presented briefly and for a more detailed overview the reader is referred to Lee [31], Wiedemann [32], Wolski [33], and the CERN Accelerator School proceedings [34]. The previously mentioned references all include the topics discussed in this chapter, and any additional sources will be indicated within the text.

3.1 Lorentz force

In circular accelerators, the guiding force for particles with velocity $\mathbf{v}$ and charge q is the Lorentz force

$$\mathbf{F}_{\mathrm{L}} = \frac{d\mathbf{p}}{dt} = q(\mathbf{v} \times \mathbf{B} + \mathbf{E}), \tag{3.1}$$

where $\mathbf{p}$ is the particle momentum, $\mathbf{B}$ the magnetic field and $\mathbf{E}$ the electric field. In high-energy particle accelerators such as the LHC, the particles are relativistic with velocities very close to the speed of light $|\mathbf{v}| \approx c$, making the force from the magnetic field considerably stronger than from the electric field. Transverse magnetic fields are therefore used for trajectory bending and beam focusing, while electric fields are used for beam acceleration.

The reference particle momentum can also be written as

$$p_0 = qB\rho, \tag{3.2}$$

where ρ is the bending radius. The quantity $B\rho$ is described as the beam rigidity, describing the strength of the magnetic field needed to change the path of the particle.

3.2 Coordinate system

To simplify the description of particle motion in an accelerator, a new coordinate system is needed. Figure 3.1 shows the Frenet-Serret curvilinear coordinate system that is commonly used in circular accelerators to describe particle motion. The longitudinal position of the particles is denoted by s, while x and y are respectively the horizontal and vertical displacement from the reference orbit, defining the transverse plane of motion. The coordinate system travels with the particles along the designed orbit trajectory in the accelerator.

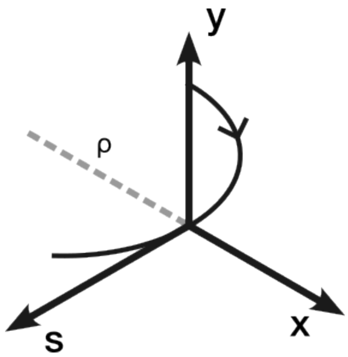

Figure 3.1. *Frenet-Serret coordinate system.*

The study of particle motion in the x and y axes is called transverse beam dynamics and accordingly to the name, longitudinal beam dynamics studies treats particle motion in the longitudinal plane. This thesis focuses on transverse beam dynamics, and the following sections describe the basic principles relating to transverse linear and nonlinear beam dynamics.

3.3 Linear beam dynamics

As the particles move through an accelerator beamline, they come across various magnetic elements that each change the particle trajectory by guiding or focusing the beam. A general way to describe transverse magnetic fields is the multipole expansion, giving information on each different multipole component on a magnetic field. For a general magnetic field $\mathbf{B}$, the multipole expansion is described as

$$B_y(x,y,s) + iB_x(x,y,s) = \sum_{n=1}^{\infty}[B_n(s) + iA_n(s)](x+iy)^{n-1}, \tag{3.3}$$

where $B_n(s)$ and $A_n(s)$ are the respective normal and skew multipole coefficients, defined in Eq. 3.4. A skew multipole of order n is rotated by $\pi/2n$ in respect to a corresponding normal multipole. The value of n denotes the type of multipole: for a dipole, $n = 1$, for quadrupoles $n = 2$ and for sextupoles $n = 3$, etc.

$$B_n(s) = \frac{1}{(n-1)!}\frac{\partial^{n-1}B_y}{\partial x^{n-1}}\bigg|_{(0,0,s)} \qquad A_n(s) = \frac{1}{(n-1)!}\frac{\partial^{n-1}B_x}{\partial x^{n-1}}\bigg|_{(0,0,s)} \tag{3.4}$$

Figure 3.2 illustrates schematically some of the commonly used magnets, of which dipoles and quadrupoles are linear elements. For sextupoles, the magnetic field changes quadratically in the transverse coordinates and is not linear, but rather the first order nonlinear element.

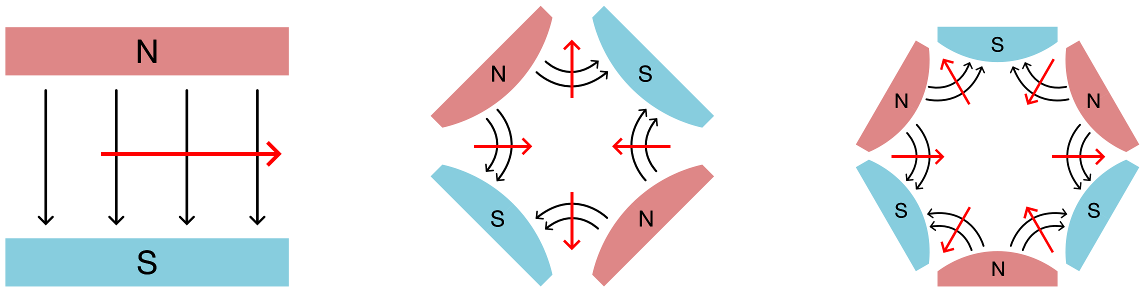

(a) *Dipole* ***(b)*** *Quadrupole* ***(c)*** *Sextupole*

Figure 3.2. *Schematic illustrations of magnetic multipoles. Black lines represent the magnetic field lines, and red lines are forces of a positively charged particle moving away from the paper towards the reader.*

Dipoles are mainly used to bend the trajectory of the beam, however they also have a weak focusing effect. The main focusing of particles in a beamline is achieved with quadrupoles.

The linear transverse motion of particles in a periodic accelerator can be described using Hill's differential equation of motion

$$u''(s) + K_u(s)u(s) = 0, \tag{3.5}$$

where $u \in \{x, y\}$ and $K_u(s)$ is the focusing effect of an element in the transverse plane u varying by the location in the machine. In the case of a drift space, $K = 0$, and with focusing and defocusing quadrupoles, the value of the focusing effect is $K > 0$ and $K < 0$, respectively.

The focusing effect for the horizontal and vertical transverse planes can be written as

$$\begin{aligned} K_x(s) &= \frac{1}{\rho(s)^2} - k_1(s) \\ K_y(s) &= k_1(s), \end{aligned} \tag{3.6}$$

where the term $k_1(s)$ is the normalized quadrupole strength

$$k_1(s) = \frac{1}{B\rho}\frac{\partial B_y(s)}{\partial x}. \tag{3.7}$$

The term $1/\rho(s)^2$ in Eq. 3.6 for the horizontal plane relates to the weak focusing caused by dipole magnets. A quadrupole magnet is focusing only in one plane, and defocusing in the other. The naming of quadrupoles is defined as the focusing property of the horizontal plane, signifying that a focusing quadrupole focuses the beam on the horizontal plane and defocuses on the vertical.

For linear optical elements, the motion of particles through an element in the beamline can be denoted using a transfer matrix $\mathbf{M}$. A more general solution to Hill's equation can be written using the transfer matrix as

$$\begin{pmatrix} u \\ u' \end{pmatrix}_s = \mathbf{M} \begin{pmatrix} u \\ u' \end{pmatrix}_0 , \tag{3.8}$$

where u_0 and u_0' are the initial values of the position and phase of the particle. Transfer matrices for a drift space, dipole, focusing quadrupole (QF) and defocusing quadrupole (QD) are expressed with

$$\mathbf{M}_{\text{drift}} = \begin{pmatrix} 1 & L \\ 0 & 1 \end{pmatrix}, \tag{3.9}$$

$$\mathbf{M}_{\text{dipole}} = \begin{pmatrix} \cos\frac{L}{\rho} & \rho\sin\frac{L}{\rho} \\ -\frac{1}{\rho}\sin\frac{L}{\rho} & \cos\frac{L}{\rho} \end{pmatrix}, \tag{3.10}$$

$$\mathbf{M}_{\text{QF}} = \begin{pmatrix} \cos\sqrt{k_1}L & \frac{1}{\sqrt{k_1}}\sin\sqrt{k_1}L \\ -\sqrt{k_1}\sin\sqrt{k_1}L & \cos\sqrt{k_1}L \end{pmatrix}, \tag{3.11}$$

$$\mathbf{M}_{\text{QD}} = \begin{pmatrix} \cosh\sqrt{|k_1|}L & \frac{1}{\sqrt{|k_1|}}\sinh\sqrt{|k_1|}L \\ \sqrt{|k_1|}\sinh\sqrt{|k_1|}L & \cosh\sqrt{|k_1|}L \end{pmatrix}, \tag{3.12}$$

where L is the length of the element and ρ is the bending radius. The transfer matrix can be constructed for a part of the beamline as the multiplication of the transfer matrices $\mathbf{M}_i$ of the individual elements i as

$$\mathbf{M} = \prod_i \mathbf{M}_i. \tag{3.13}$$

For a full revolution of the machine, the transfer matrix is called the one-turn map, and it is denoted as

$$\mathbf{M}_{\mathrm{OTM}} = \mathbf{M}_n \mathbf{M}_{n-1} \cdots \mathbf{M}_2 \mathbf{M}_1, \tag{3.14}$$

where $\mathbf{M}_i$ is the transfer matrix of a single element and n is the total number of elements. The change of coordinates for a single particle over one revolution can then be determined by

$$\begin{pmatrix} u \\ u' \end{pmatrix}_{s_0+C} = \mathbf{M}_{\mathrm{OTM}} \begin{pmatrix} u \\ u' \end{pmatrix}_{s_0}, \tag{3.15}$$

where C is the circumference of the ring.

3.3.1 Courant-Snyder parameters

A solution for Hill's equation can be expressed as

$$\begin{aligned} u(s) &= \sqrt{2J_u\beta_u(s)}\cos\left(\phi_u(s) + \phi_{u,0}\right), \\ u'(s) &= -\sqrt{\frac{2J_u}{\beta_u(s)}}\left(\sin(\phi_u(s) + \phi_{u,0}) + \alpha_u(s)\cos(\phi_u(s) + \phi_{u,0})\right), \end{aligned} \tag{3.16}$$

where J is the betatron action, $\beta_u(s)$ the betatron function, $\phi_u(s)$ the phase advance and $\alpha_u(s)$ the alpha function. The action J_u characterises the maximum amplitude of the betatron oscillation.

The betatron function or β-function $\beta_u(s)$ is a property of the lattice that describes the envelope of oscillation amplitudes of particles, relating to the maximum amplitude for a single particle trajectory at location s in the beamline. The oscillating nature of the β-function is due to the periodic focusing and defocusing quadrupoles around the machine, as illustrated in Fig. 3.3.

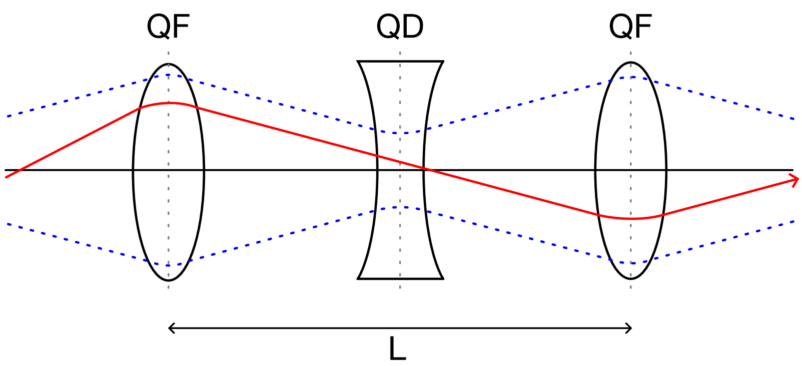

Figure 3.3. *Schematic illustration of a typical FODO cell of length L with the beam envelope in blue and an example trajectory in red.*

The simplest strong focusing lattice is the FODO cell, consisting of a focusing quadrupole, drift space, defocusing quadrupole and a second drift, visualised in Fig. 3.3. The transfer matrix for a FODO cell is

$$\mathbf{M}_{\mathrm{FODO}} = \mathbf{M}_{\mathrm{QF}} \cdot \mathbf{M}_{\mathrm{drift}} \cdot \mathbf{M}_{\mathrm{QD}} \cdot \mathbf{M}_{\mathrm{drift}}. \tag{3.17}$$

In synchrotrons, the drift spaces in FODO cells located in the arcs are replaced by bending dipole magnets. Close to the Interaction Points (IPs), very small beam sizes are needed to produce the most collisions. Thus the quadrupole magnets are placed in triplets to first rapidly increase and decrease the value of the β-function. The value of the β-function at the IPs is normally referred to as the β^*.

The term $\phi_u(s)$ is called the phase advance, which is the difference of the betatron phase functions of two points. The phase advance can be expressed with the β-function with

$$\phi_u(s) = \phi_u(s_1) - \phi_u(s_0) = \int_{s_0}^{s_1} \frac{1}{\beta_u(s)} \mathrm{d}s. \tag{3.18}$$

The α-function in the derivative function of Eq. 3.16 can be defined as the derivative of the β-function with

$$\alpha_u(s) = -\frac{\beta_u'(s)}{2}. \tag{3.19}$$

In addition, the γ-function is defined as

$$\gamma_u(s) = \frac{1 + \alpha_u^2(s)}{\beta_u(s)}, \tag{3.20}$$

describing beam divergence. The parameters $\alpha_u(s)$, $\beta_u(s)$, $\gamma_u(s)$ and $\phi_u(s)$ are called the Courant-Snyder or Twiss parameters, and the one-turn map can be expressed using them as [35]

$$\mathbf{M}_{\mathrm{OTM}} = \begin{pmatrix} \cos(2\pi Q_u) + \alpha_u \sin(2\pi Q_u) & \beta_u \sin(2\pi Q_u) \\ -\gamma_u \sin(2\pi Q_u) & \cos(2\pi Q_u) - \alpha_u \sin(2\pi Q_u) \end{pmatrix}. \tag{3.21}$$

The number of betatron oscillations in one revolution is described using a variable called tune Q_u, and it is defined with

$$Q_u = \frac{1}{2\pi} \oint_C \frac{1}{\beta_u(s)} ds. \tag{3.22}$$

The working point of a machine is defined with the horizontal and vertical tunes as (Q_x, Q_y), and is usually denoted with only the fractional part of the tune. The tune is one of the most important parameters of an accelerator, and needs to be selected carefully in order to avoid resonances.

3.3.2 Phase space and emittance

Particle beams can be characterized using the phase space (u, p_u), where each point represents a single particle. For systems consisting of only linear elements, the particle distribution in phase space is an ellipse, as visualised in Fig. 3.4. According to the Liouville theorem, the volume of the ellipse in the phase space for a closed system is constant under the influence of conservative forces. The area of the phase space is defined by the beam emittance with $A = \pi\varepsilon_u$.

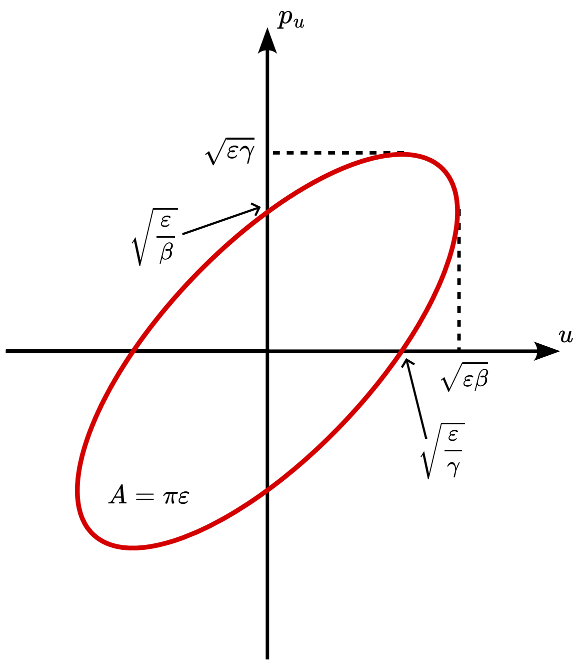

Figure 3.4. *Phase space ellipse in the (u, p_u) space with characteristic coordinates of the ellipse represented with Twiss parameters.*

The emittance or the Courant-Snyder invariant ε can be used to characterize the ellipse equation defining the phase space as

$$\varepsilon_u = \gamma_u(s)u(s)^2 + 2\alpha_u(s)u(s)p_u(s) + \beta_u(s)p_u(s)^2. \tag{3.23}$$

When a beam is accelerated, the Liouville theorem is not applicable since the system is no longer closed. The emittance ε_u does not remain constant, and instead the invariant quantity is the normalised emittance $\varepsilon_u^{\mathrm{norm}}$, defined as

$$\varepsilon_u^{\text{norm}} = \beta_{\text{rel}}\gamma_{\text{rel}}\varepsilon_u, \tag{3.24}$$

where β_{rel} and γ_{rel} are relativistic parameters. The geometric emittance of a single particle relates to the action J, an invariant that defines the transverse amplitude of the particle as

$$\varepsilon_u = 2J_u. \tag{3.25}$$

The amplitude of the beam in the transverse plane can be defined using the emittance as

$$\mathcal{A}_u(s) = \sqrt{\varepsilon_u^{\text{beam}}\beta_u(s)}, \tag{3.26}$$

where $\varepsilon_u^{\text{beam}}$ describes the emittance of all particles in a beam, as the mean of all the individual actions.

3.3.3 Dispersion and chromaticity

Particle dispersion arises from the variation of the particle's actual momentum compared to the nominal momentum p_0. In real life, the energy and momentum of particle beams is distributed instead of being constant. This means that the energy of the particle is different, and it bends differently depending on its energy. The relative momentum deviation for a particle with momentum of $p \neq p_0$ is

$$\delta_p = \frac{p - p_0}{p_0} \tag{3.27}$$

and the deviation from the reference orbit due to dispersion can be expressed with

$$\Delta u_{\text{disp}} = D_u(s)\delta_p, \tag{3.28}$$

where $D_u(s)$ is the dispersion function.

Additionally, deviations in the particle momentum cause changes in the effective focusing strength of quadrupole magnets. The variation of the strength results in the particles experiencing different focusing, leading to variation of the tune with energy. The variation is called chromaticity, and it is defined by

$$Q'_u = \frac{\Delta Q_u}{\delta_p}, \tag{3.29}$$

where ΔQ_u is the tune shift and δ_p is the relative momentum deviation. The natural chromaticities are always negative, and the circumference of the accelerator has an effect on the natural chromaticity.

3.4 Nonlinear beam dynamics

In addition to linear magnets, particle accelerators have higher-order multipolar magnets to improve the quality of the beam even further. The lowest higher-order magnetic multipole, the sextupole, is illustrated in Fig. 3.2c. Sextupoles are used for correcting chromatic aberrations. Nonlinearities arise not only from the higher-order multipolar magnets, but also higher-order multipole components from dipoles and quadrupoles, resulting from misalignments and magnetic errors. The effect on nonlinearities in a particle accelerator can have a significant impact on operation. Extensive research is currently being performed to better understand the measurement and correction of nonlinear beam dynamics. Since this thesis focuses on linear beam dynamics, only a very brief overview of nonlinearities in particle accelerators is discussed. A more in-depth description of nonlinear beam dynamics can be found in Refs. [11, 36].

Nonlinearities distort the phase space, making the action $2J_u$ no longer constant. The complex normalized coordinates can be described using the action J_u and phase ϕ_u with

$$h_{u,\pm} = \hat{u} \pm i\hat{p}_u = \sqrt{2J_u}e^{\mp i(\phi_u+\phi_{u,0})}. \tag{3.30}$$

A coordinate transformation is needed to describe motion in a circular phase space with nonlinear sources present. The transformation from normalized coordinates to normal form coordinates can be performed using the exponential Lie operator as

$$\zeta_{u,\pm} = e^{-:F:}h_{u,\pm} = \sqrt{2I_u}e^{\mp i(\psi_u+\psi_{u,0})}, \tag{3.31}$$

where I_u is the new motion invariant and ψ_u the new phase. The motion of transverse oscillations of the N^{th} turn can be expressed with

$$\begin{aligned} \zeta_{x,-}(N) =& \sqrt{2I_x}e^{i(2\pi Q_x N+\psi_{x0})} \\ & - 2i\sum_{jklm} j f_{jklm}(2I_x)^{\frac{j+k-1}{2}}(2I_y)^{\frac{l+m}{2}} \\ & \cdot e^{i[(1-j+k)(2\pi Q_x N+\psi_{x0})+(m-l)(2\pi Q_y N+\psi_{y0})]}, \end{aligned} \tag{3.32}$$

where the first term describes the linear motion and the second term includes the nonlinear contributions. The f_{jklm} coefficients describe resonance driving terms (RDTs) with

$$f_{jklm} = \frac{h_{jklm}}{1 - e^{2\pi i[(j-k)Q_x + (l-m)Q_y]}}, \tag{3.33}$$

where h_{jklm} are the Hamiltonian coefficient terms including the contribution of all multipoles of order $n = j + k + l + m$. For a certain value of the tunes Q_x and Q_y, Eq. 3.33 shows that the f_{jklm} coefficients diverge. The resonance driving terms diverge when a resonance is reached, defined by the equation

$$(j - k)Q_x + (l - m)Q_y = p, \quad p \in \mathbb{Z}. \tag{3.34}$$

The working point of an accelerator needs to be chosen carefully to avoid resonances. Resonance lines up to the fifth order ($n = 5$) are shown in Fig. 3.5, with working points used in this thesis indicated.

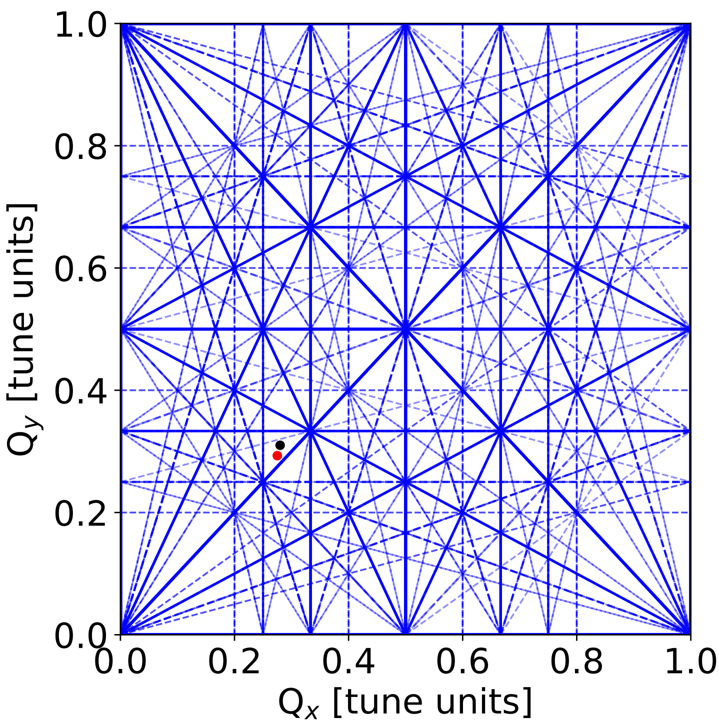

Figure 3.5. *Tune diagram showing all resonance lines up to the fifth (decapolar) order. The working points used in this thesis are indicated by the red ($Q_x = 0.275, Q_y = 0.293$) and black ($Q_x = 0.280, Q_y = 0.310$) dots. Diagram made using [37].*

A spectral component can be defined for each resonance, and their amplitude in the horizontal and vertical planes are given by

$$\begin{aligned} H(1 - j + k, m - l) &= 2j|f_{jklm}|(2I_x)^{\frac{j+k-1}{2}}(2I_y)^{\frac{l+m}{2}} \\ V(k - j, m - l + 1) &= 2l|f_{jklm}|(2I_x)^{\frac{j+k}{2}}(2I_y)^{\frac{l+m-1}{2}} \end{aligned} \tag{3.35}$$

As an example, $H(2, 0)$ corresponds to the line $2Q_x$ in the horizontal frequency spectrum.

3.5 Coupling

Betatron coupling refers to the dependency of the horizontal and vertical transverse motion of particles. The preferred behaviour in particle colliders such as the LHC is the opposite so that the motion is uncoupled, but several factors may introduce coupling in an accelerator. The main contribution of coupling in the LHC arises from skew quadrupolar fields due to mounting errors of normal quadrupoles.

In the case of uncoupled motion, two independent 2×2 matrices could be used to describe the motion. If betatron coupling is present, the transverse motion is described by

$$\begin{pmatrix} x \\ p_x \\ y \\ p_y \end{pmatrix} = \begin{pmatrix} \mathbf{P} & \mathbf{p} \\ \mathbf{q} & \mathbf{Q} \end{pmatrix} \begin{pmatrix} x \\ p_x \\ y \\ p_y \end{pmatrix}_0 , \tag{3.36}$$

where $\mathbf{P}$, $\mathbf{p}$, $\mathbf{q}$ and $\mathbf{Q}$ are 2×2 matrices. When there is no coupling, $\mathbf{p}$ and $\mathbf{q}$ are 0.

Linear coupling drives the resonances $(Q_x - Q_y) = p$ and $(Q_x + Q_y) = p$, with $p \in \mathbb{Z}$. The coupling needs to be corrected in order to not disturb the tune feedback and drive the tunes into the resonances, causing beam instabilities [38].

3.6 Amplitude detuning

Amplitude detuning relates to the tune dependency as a function of the oscillation amplitude. For studying nonlinearities in a particle accelerator, amplitude detuning is one of the main observables as it is easily affected by errors in nonlinear magnets, in particular octupoles and dodecapoles. The Taylor expansion stated up to the second order for the tune Q_u around the unperturbed tune Q_{u0} is expressed with

$$\begin{aligned} Q_u(2J_x, 2J_y) = Q_{u0} &+ \frac{\partial Q_u}{\partial(2J_x)} 2J_x + \frac{\partial Q_u}{\partial(2J_y)} 2J_y \\ &+ \frac{1}{2!}\left(\frac{\partial^2 Q_u}{\partial(2J_x)^2}(2J_x)^2 + 2\frac{\partial^2 Q_u}{\partial(2J_x)\partial(2J_y)} 2J_x 2J_y + \frac{\partial^2 Q_u}{\partial(2J_y)^2}(2J_y)^2 \right) + \ldots , \end{aligned} \tag{3.37}$$

where Q_u can either be Q_x or Q_y. The first order detuning terms are generated by octupoles and sextupoles, and the second order terms arise from higher order magnetic multipoles. Amplitude detuning is a widely researched issue in particle accelerators [39, 40], since changes in the tune can cause particle losses and the reduction of dynamic aperture by approaching the resonances faster.

4. OPTICS MEASUREMENTS IN THE LHC

The functioning principle of magnets of different order multipoles in accelerators resemble lenses used to guide and focus light beams, and therefore the measurement of the beam size or phase is referred to as optics measurements. Optics deviations have a direct effect on the machine performance and achieved luminosity, as the luminosity depends on the β-functions at the IPs. If the propagation of the beams is perturbed largely and the optics are not in good control, the machine will not behave as designed. The changes in the machine conditions has an impact on all accelerator systems, i.e. instrumentation and collimation, and the accelerator may not be operated for safety reasons. Optics deviations result in changes in β-functions and phase advances compared to the designed and modelled machine, resulting in breaking of symmetries in optics. This reduces beam control, feedback controls and instability mitigations. Good control of machine optics is therefore critical for the LHC operation and requires accurate optics measurements and corrections.

Typical optics measurements in particle colliders are performed using pilot bunches that have a low intensity. The bunches are excited or kicked, providing a coherent transverse oscillation to the beam. This long term oscillation is recorded using Beam Position Monitors (BPMs) that are located around the ring to determine the transverse position of the beam throughout the machine. Spectral analysis of the provided turn-by-turn data is important for revealing the main and secondary modes of motion. From the main betatron mode, the optics parameters β and ϕ can be calculated. A more detailed description of the measurement process is explained in the following sections.

4.1 Machine setup

Optics measurements are performed using up to three low-intensity pilot bunches with an intensity of around 1×10^{10} protons per bunch. This low-intensity bunch is used for machine protection reasons to limit particle losses when exciting the beam. For other machine parameters, the collimators are set to coarse settings providing a larger physical aperture to allow for large beam excitations with minimal losses to the beams and to prevent machine protection dumps.

The quality of the optics in the machine needs to be validated at all points in the operational cycle. Therefore optics measurements are performed at injection, during the energy ramp-up, at top energy and during various points of the squeeze.

4.2 Beam excitation methods

Beam-based optics measurements in the LHC are based on exciting the beam using an oscillating dipolar field. The excitation provides a transverse betatronic oscillation around the closed orbit. In order to measure optics parameters such as the β-function and phase, the amplitude of the oscillation needs to be sufficient to be recorded by BPMs around the machine. The transverse oscillation is created by exciting the beam using a frequency close to the natural tune. Two dedicated elements can be used in the LHC for such excitations, the ac dipole and the ADT.

Typically, linear and nonlinear optics measurements in the LHC are performed using an ac dipole [7–11, 41–43] which is a strong dipole magnet with an oscillating field. The provided transverse beam excitation is long-term and coherent, improving the spectral resolution of the measurement. In addition, the excitation amplitude is ramped up and down slowly, as seen in Fig. 4.1. This makes the excitation adiabatic, not causing significant emittance growth [44], and ensuring that the beam can be reused after the excitation.

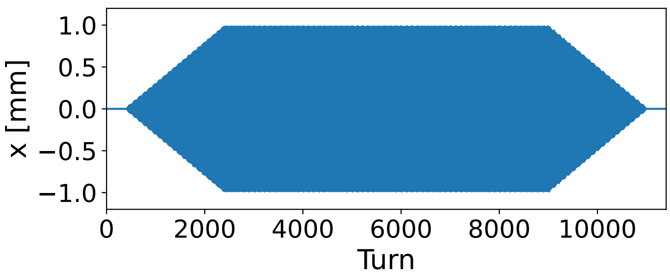

Figure 4.1. *Simulation of turn-by-turn transverse position data from an ac dipole excitation. The amplitude is ramped up for 2000 turns, held at flat top for 6600 turns and ramped down for 2000 turns.*

While the ac dipole provides a large oscillation amplitude, it can be used for only a limited duration due to heating of the electronics. Currently the maximum flat top excitation with the ac dipole in the LHC is 6600 turns. Due to the cool-down period, reloading the ac dipole takes approximately one minute.

An alternative excitation method for the LHC is using the ADT to provide a transverse oscillation to the beam. The ADT is a versatile system built initially for injection oscillation damping and instability feedback. During Run 2, the ADT was upgraded to provide an ac dipole-like transverse beam excitation [13, 45]. Since August 2017, the system has been included in the operational procedure for the calculation of coupling corrections at the start of each fill [46].

The excitation strength of the ADT is sufficient for correcting the coupling, but not for detailed and accurate optics measurements with 6600 turns. As the excitation strength cannot be increased with the current measurement software, other approaches for improving the spectral resolution need to be considered. The ADT provides turn-by-turn data with an unlimited duration. Increasing the number of turns to the limits of the BPMs offers an important improvement in the signal-to-noise ratio, and consequently in the spectral resolution. Furthermore, consecutive measurements with the ADT can be performed quickly, since the primary limitation originates from the BPM buffers which have a fast reloading time. In addition, the ADT can be used in operational conditions with high-intensity beams, and single bunches within bunch trains of 25 ns can be excited [45]. The ac dipole can only be used with single low-intensity bunches due to machine protection reasons.

Figure 4.2 shows the most notable differences from a turn-by-turn measurement at injection energy between the two beam excitation methods. The ADT has a lower excitation amplitude than the ac dipole, but the ADT data acquisition is recorded for a longer time duration.

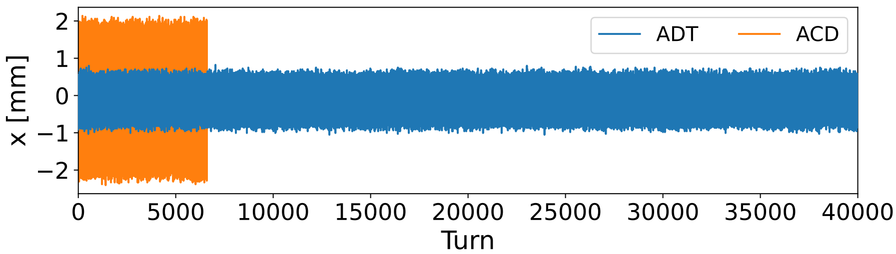

Figure 4.2. *Turn-by-turn data comparison between an ADT measurement with 40 000 turns and an ac dipole (ACD) measurement with 6600 turns for Beam 1.*

The transverse position of the bunch through the ring, excluding the ramp-up and the ramp-down, is recorded with Beam Position Monitors that are discussed in more detail in the following section.

4.3 Beam Position Monitors

Beam Position Monitors (BPMs) [47] are beam instrumentation tools that provide transverse horizontal and vertical position data of the beam in the accelerator beamline. BPMs are used for measuring the transverse propagation of the beam, and in circular accelerators they are used for calculating the closed orbit. In addition, BPMs are used to measure the transverse position of a bunch in a specific location at each turn, providing turn-by-turn data. In the LHC, approximately 525 dual-plane BPMs per beam are used to measure the transverse position of the beam [14].

Figure 4.3 illustrates a typical, button-type BPM used in the LHC. The BPM consists of four round metallic electrodes, arranged symmetrically along the horizontal and vertical axes. As the beam propagates through the BPM, it induces a mirrored electric charge in each electrode, and the difference in voltage between the two opposing pickups indicates the transverse position of the beam at the location of the BPM. The transverse position is recorded for each turn, and the obtained turn-by-turn data is a discrete time oscillation signal of the beam position at the location of each BPM.

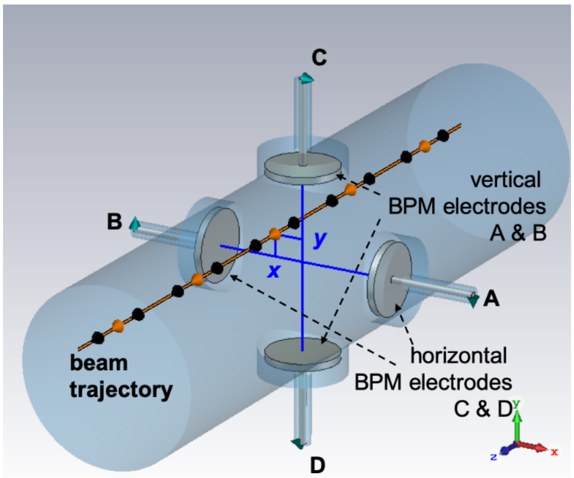

Figure 4.3. *Illustration of a button-type Beam Position Monitor [47].*

The amplitude of the oscillation needs to be sufficient for the BPMs to observe the transverse position. In addition, a larger oscillation amplitude provides a better signal-to-noise ratio. The BPM buffers limit the number of turns to 40 000. The high limit of recorded turns is of great benefit for the ADT and the first ADT measurements utilising the higher number of turns are presented in this thesis.

4.4 Spectral analysis of BPM data

Information about the oscillation modes of the beam is revealed by performing a Fourier transform on the recorded turn-by-turn data of each BPM. Figure 4.4 shows the normalized horizontal frequency spectrum from an ac dipole measurement obtained at injection energy in 2023. The main mode of the oscillation is the betatron oscillation with information about the amplitude and the phase of the beam. From these, the β-function can be reconstructed, as described in the following section. The secondary modes in Fig. 4.4 are due to nonlinear contributions from the machine, discussed in more detail in Chapter 3.4.

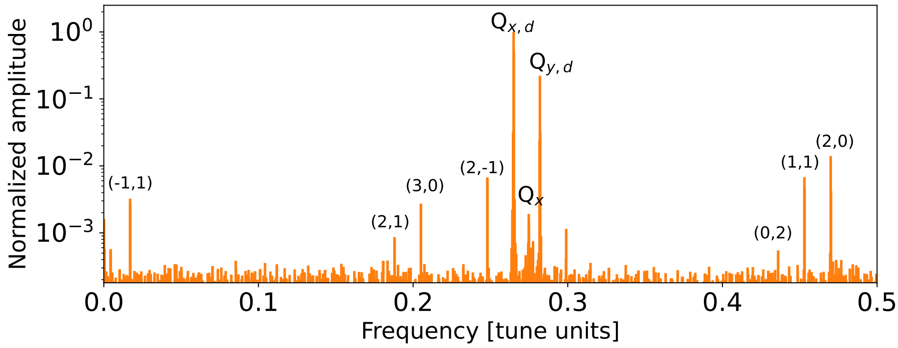

Figure 4.4. *Horizontal frequency spectrum of an ac dipole measurement taken in 2023. The natural tune line is indicated with Q_x, and the driven or main tune lines with $Q_{x,d}$ and $Q_{y,d}$. The lines (m, n) correspond to frequencies $mQ_{x,d} + nQ_{y,d}$, where $m, n \in \mathbb{N}$, arising from nonlinear contributions.*

All analysis done in this thesis is performed using the OMC3 software, developed by the OMC (Optics Measurements and Corrections) -team at CERN [48]. The frequency analysis is done using the `harpy`-package [49]. It is an efficient tool that cleans the noisy turn-by-turn data and removes outlier BPMs, and computes the frequency spectrum for all individual BPMs using zero-padded real Fast Fourier Transform (RFFT).

4.5 Optics

For calculating the β-functions from the measured phase advances, one approach is to use the 3-BPM method [50]. It uses the phase advances of three nearby BPMs to calculate the β function at the probed BPM using

$$\beta_i = \beta_i^{\mathrm{mod}} \frac{\cot\phi_{ij} - \cot\phi_{ik}}{\cot\phi_{ij}^{\mathrm{mod}} - \cot\phi_{ik}^{\mathrm{mod}}}, \tag{4.1}$$

where i, j and k denote the three consecutive BPMs and ϕ_{ij} is the phase advance between BPMs i and j. Values indicated with the superscript mod correspond to phase advances from the model. The model of the LHC is constructed with MAD-X (Methodical Accelerator Design) [51], a design program for accelerators developed at CERN, specifically for the technical design of the LHC. The 3-BPM method is visualised in Fig. 4.5. A defect in this method is the divergence of the equation for phase advances close to $n\pi$, $n \in \mathbb{N}$, enhancing phase measurement errors.

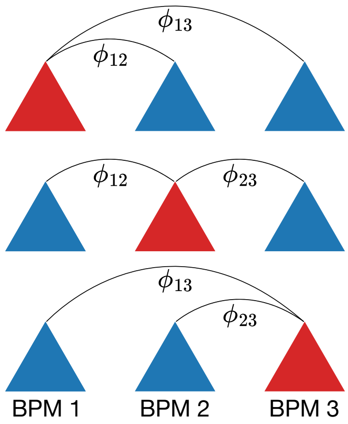

Figure 4.5. *Visualisation of the 3-BPM method. The probed BPM is shown in red.*

In the LHC arcs the phase advance between two consecutive BPMs is approximately $\pi/4$, which can become an issue when using the 3-BPM method. In order to improve measurement accuracy and take unsuitable phase advances into account, a new method called the N-BPM method was developed [52]. With it, BPMs can be skipped around the probed BPM to utilise the BPMs with optimal phase advances and avoid the unsuitable ones. Figure 4.6 shows the basic principle of the N-BPM method.

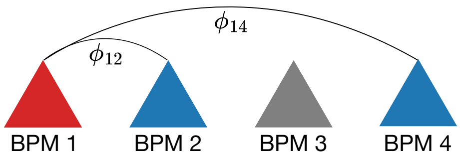

Figure 4.6. *Visualisation of the N-BPM method. The probed BPM is shown in red, and the BPM shown in gray is skipped.*

The measured β-function can then be calculated for the lth combination with

$$\beta_l(s_i) = \frac{\cot \phi_{ij_l} - \cot \phi_{ik_l}}{\cot \phi_{ij_l}^{\mathrm{mod}} - \cot \phi_{ik_l}^{\mathrm{mod}}} \beta^{\mathrm{mod}}(s_i), \tag{4.2}$$

where the final β-function is obtained from a weighted sum from multiple BPM combinations as

$$\beta(s_i) = \sum_l \beta_l(s_i) g_l, \tag{4.3}$$

where g_l are weights.

The method improved the precision of β-function measurements, specially in the Interaction Region (IRs) around the IPs, by skipping the neighboring BPMs that have a phase advance of π, resulting for the 3-BPM method to fail. However, the original N-BPM method calculates the statistical uncertainties analytically, and the systematic errors are evaluated from Monte Carlo simulations. For obtaining a good precision, the number of simulations needed to be performed takes time.

The analytical N-BPM method [53] was developed as an improvement to the original N-BPM method by reducing the processing time for measurements by calculating also the systematic uncertainties analytically. The original N-BPM method did not take into action additional elements between BPMs, and the equation for the β-function in the analytical N-BPM methods implements quadrupolar errors, making the calculation more accurate. The β-function is calculated with

$$\beta(s_1) = \frac{\cot\phi_{12} - \cot\phi_{13}}{\cot\phi_{12}^{\mathrm{mod}} - \cot\phi_{13}^{\mathrm{mod}} + \bar{h}_{12} - \bar{h}_{13}} \beta^{\mathrm{mod}}(s_1) + O(\delta K_1^2), \tag{4.4}$$

where

$$\bar{h}_{ij} = \frac{\sum\limits_{i<w<j} \beta_w^{\mathrm{mod}} \delta K_{w,1} \sin^2\phi_{wj}^{\mathrm{mod}}}{\sin^2\phi_{ij}^{\mathrm{mod}}}. \tag{4.5}$$

A good indicator of the quality of the linear optics in an accelerator is the β-beating, which is defined as the relative deviation of the measured β-function from the β-function from the model. The β-beating can be defined as

$$\frac{\Delta\beta_u(s)}{\beta_u^{\mathrm{mod}}(s)} = \frac{\beta_u(s) - \beta_u^{\mathrm{mod}}(s)}{\beta_u^{\mathrm{mod}}(s)}, \tag{4.6}$$

where values indicated with the superscript mod correspond to β-functions from the model, and $u \in \{x, y\}$. In the LHC, the maximum tolerable peak β-beating at injection needs to be below 14 % and 16 % for the horizontal and vertical plane respectively, and at collision optics 15 % and 19 % [54]. In operation, the β-beating needs to be even lower in order to achieve the luminosity requirements. During the 2023 commissioning, the peak β-beating was reduced to below 10 % for both beams and both planes [10].

5. EXPERIMENTAL RESULTS

This chapter presents the results of ADT optics measurements in the LHC performed in 2023. Measurements were taken during beam commissioning and dedicated experiments in Machine Development (MD) periods. The results presented are from measurements taken at injection energy (450 GeV) and at top energy (6.8 TeV) with low-intensity bunches in different machine conditions.

The aim of the studies conducted in this thesis is to demonstrate that the ADT can provide equivalent performance to the ac dipole for optics measurements. ADT measurements will therefore be compared to ac dipole measurements taken at the same machine configuration. First, analysis of ADT measurement data taken during routine operation in 2022 is presented. Based on the results, measurements were performed in 2023 with improvements to the measurement conditions. ADT measurements were performed to measure the linear optics and to compare it to the ac dipole on five separate occasions, and the ADT measurement conditions for each occasion are summarized in Table 5.1. The actions $\sqrt{2J}$ for each occasion are calculated as the average of multiple measurements with the same set kick amplitude.

5.1 Linear optics at injection

This chapter presents linear optics measurements taken with the ADT in three occasions. As a reference, 2022 ADT excitations are analysed and based on those results, improvements are made to measurements performed in 2023 in two separate occasions.

5.1.1 Spectral resolution

Routine beam excitations have been performed with the ADT since August 2017 for measuring and correcting the coupling in the LHC [46]. For this type of measurement, 6600 turns of turn-by-turn data from BPMs is sufficient for a coupling correction of the level of $|C-| \approx 10^{-3}$. Data with the ADT taken in November 2022 for coupling corrections was analysed in this thesis to check the optics. Measurements were taken in the timespan of three days for 13 different fills, with one or two measurements per fill depending on if a coupling correction was needed. The natural and driven tunes for these measurements

Table 5.1. *Measurement conditions for ADT measurements analysed for linear optics in this thesis. The measurements are sorted by their order of first appearance in the thesis.*

	Measurement				
	2022	14/06/2023	30/08/2023	31/08/2023	08/06/2023
Energy [GeV]	450	450	450	6800	6800
$\beta^*_{\mathrm{IP1,IP5}}$ [m]	11	11	11	0.3	120
Turns	6600	28 500	40 000	40 000	40 000
Q_x	0.275	0.275	0.280	0.280	0.280
Q_y	0.293	0.293	0.310	0.310	0.310
Q_x^{ADT}	0.265	0.265	0.270	0.270	0.270
Q_y^{ADT}	0.308	0.303	0.321	0.325	0.320
ΔQ_x	-0.010	-0.010	-0.010	-0.010	-0.010
ΔQ_y	+0.015	+0.010	+0.011	+0.015	+0.010
B1 $\sqrt{2J_x}$ $[10^{-5}$ m]	2.870	4.778	4.585	0.543	1.068
B1 $\sqrt{2J_y}$ $[10^{-5}$ m]	1.050	2.978	2.545	0.306	0.800
B2 $\sqrt{2J_x}$ $[10^{-5}$ m]	3.697	7.025	7.340	0.483	0.965
B2 $\sqrt{2J_y}$ $[10^{-5}$ m]	1.653	4.316	3.805	0.353	0.944

were $Q_x = 0.275$ and $Q_x^{ADT} = 0.265$ for the horizontal plane and $Q_y = 0.293$ and $Q_y^{ADT} = 0.308$ for the vertical plane.

Figures 5.1 and 5.2 show the normalized horizontal and vertical frequency spectrum for Beam 1 and Beam 2 from a single BPM for a single ADT measurement taken in 2022, compared to a typical ac dipole (ACD) measurement. The excitation amplitude of the ac dipole is higher than the ADT, resulting in a lower noise level in the normalized frequency spectrum with respect to the main mode. In addition, ac dipole measurements show several secondary lines that are not visible in the ADT frequency spectrum. When comparing the ADT measurements, the noise floor of the vertical plane is higher than the horizontal plane, and Beam 2 has a lower noise floor compared to Beam 1. As expected, larger oscillation amplitudes improve the signal-to-noise ratio.

An analysis of phase error of the main mode with relation to the oscillation amplitude was performed to better quantify the effect of amplitude on ADT measurements. The error on the phase advance of the betatronic oscillation was calculated from turn-by-turn data for a single BPM. For each measurement, the average error of the phase advance over all BPMs was calculated. Figure 5.3 presents the phase error as a function of the action $\sqrt{2J}$ or the oscillation amplitude for ADT and ac dipole with a single excitation per point.

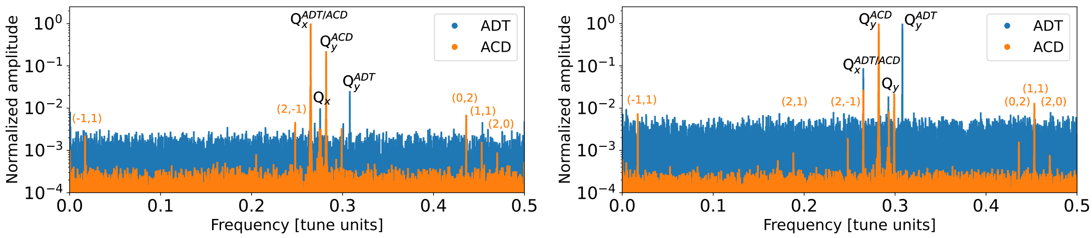

Figure 5.1. *Horizontal (left) and vertical (right) frequency spectra of Beam 1 at BPM.10L4.B1 at injection energy for ADT and ac dipole measurements taken with ADT excitation of 6600 turns.*

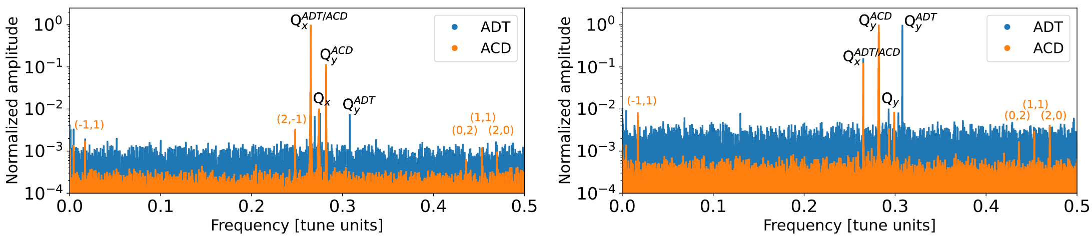

Figure 5.2. *Horizontal (left) and vertical (right) frequency spectra of Beam 2 at BPM.10L4.B2 at injection energy for ADT and ac dipole measurements taken with ADT excitation of 6600 turns.*

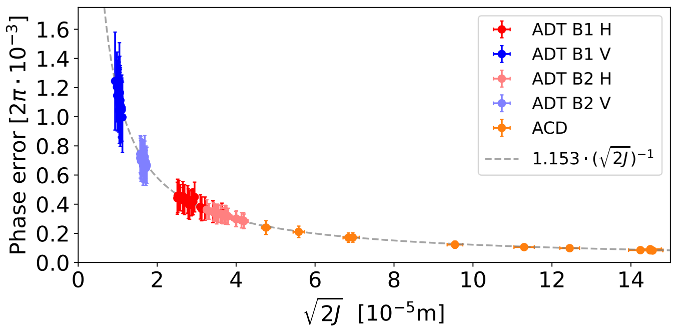

Figure 5.3. *Phase error as a function of oscillation amplitude for ADT and ac dipole excitations at injection.*

Excitation for the ac dipole is well controlled, and the kick amplitude can be set different for each beam and each plane. For the ADT, the software used to control ADT excitations sets the same amplitude for both planes of both beams. However, the resulting amplitude is not equal by beam or plane as seen in Fig. 5.3. The action or the oscillation amplitude directly relates to the noise level, and the actions seen in Fig. 5.3 agree with the qualitative observations of noise floors in the normalized frequency spectra in Figs. 5.1 and 5.2. Figure 5.3 shows that excitations in the horizontal plane have a larger oscillation amplitude compared to the vertical plane. Beam 2 has a higher excitation amplitude than Beam 1 in both planes, as observed with the calculated actions in Table 5.1. The variation in oscillation amplitudes between the different planes and beams needs to be studied in more detail to understand the issue.

Figure 5.3 shows that when the oscillation amplitude of the excitation increases, the phase error decreases relative to the inverse of the oscillation amplitude. With 6600 turns, the two excitation methods set on the same curve.

In order to decrease the phase error for ADT measurements to obtain a comparable resolution to the ac dipole, two upgrades can be followed. The kick amplitude can be increased, or the number of turns can be increased. For the ADT the excitation strength is limited, however the length of the coherent transverse excitation is unlimited. The limitation for the measurements arises from the BPMs that can only acquire data up to around 40 000 turns while maintaining stable buffers. In addition, the working point can be modified to excite the beam closer to the resonance and thus acquire a higher oscillation amplitude.

ADT measurements were taken at injection with an increased number of turns at two separate occasions. On June 14, 2023, optics measurements with the ADT were performed at injection energy using a single pilot bunch and 28 500 turns of transverse oscillations during a Machine Development campaign MD9549 [55]. The natural and driven tunes for these measurements were $Q_x = 0.275$ and $Q_x^{\mathrm{ADT}} = 0.265$ for the horizontal plane and $Q_y = 0.293$ and $Q_y^{\mathrm{ADT}} = 0.303$ for the vertical plane. Figures 5.4 and 5.5 compare the obtained horizontal and vertical frequency spectra of an ADT and an ac dipole measurement for Beam 1 and Beam 2, respectively.

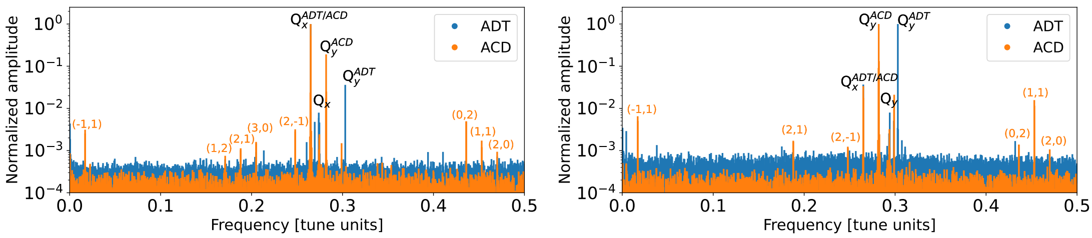

Figure 5.4. *Horizontal (left) and vertical (right) frequency spectra of Beam 1 at BPM.10L4.B1 at injection energy for ADT and ac dipole measurements with ADT excitation of 28 500 turns.*

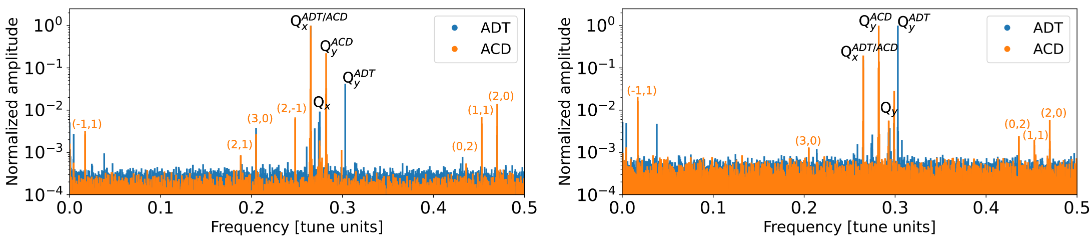

Figure 5.5. *Horizontal (left) and vertical (right) frequency spectra of Beam 2 at BPM.10L4.B2 at injection energy for ADT and ac dipole measurements with ADT excitation of 28 500 turns.*

Now both the ADT excitation amplitude and the number of turns are higher than in measurements done in 2022, and the noise floors agree better with the corresponding ac dipole measurements. Higher noise floor in a normalized frequency spectrum directly corresponds to a lower kick amplitude. In addition, reducing the tune split between the natural and driven tune in the vertical plane increased the oscillation amplitude, as seen in Table 5.1. Some variation of the oscillation amplitudes can still be seen between different beams and planes for ADT measurements, as previously observed with beam excitations with the ADT. The greatest difference between the noise floors of the two excitation methods can be seen for the vertical plane of Beam 1. A possible explanation to this may be the low excitation amplitude of the ADT in the vertical plane of Beam 1. Further research is needed to characterise the difference in oscillation amplitudes between the different beams and planes.

LHC operation in 2023 was interrupted due to a quench of an inner triplet magnet [56], causing extreme mechanical stress to the magnet itself and as a result, helium gas leaked to the insulation vacuum. The leak repair and cooling of the magnets back to their superconducting state of this incident took time, and recommissioning was needed at the end of August to ensure safe operation conditions and measurement reproducibility.

ADT measurements were taken during the optics recommissioning on August 30, 2023 using a single pilot bunch with 40 000 turns. The working point for these measurements differs from the earlier introduced measurements at injection, with the natural and driven tunes being $Q_x = 0.280$ and $Q_x^{\mathrm{ADT}} = 0.270$ for the horizontal plane and $Q_y = 0.310$ and $Q_y^{\mathrm{ADT}} = 0.321$ for the vertical plane. The horizontal and vertical frequency spectra of a single ADT measurement compared to an ac dipole measurement for both beams are shown on Figs. 5.6 and 5.7. Now the set excitation amplitude is equal to measurements during MD9549, but the number of turns is even higher, resulting in a better match of the noise floor between the ADT and the ac dipole for the horizontal plane of both beams. As for the vertical plane, the noise floor of the ADT remains higher than of the ac dipole, agreeing with the previous measurements. In addition, the improvement on the signal-to-noise ratio unveils visible secondary modes in the ADT frequency spectrum that are discussed in more detail in Chapter 5.4.

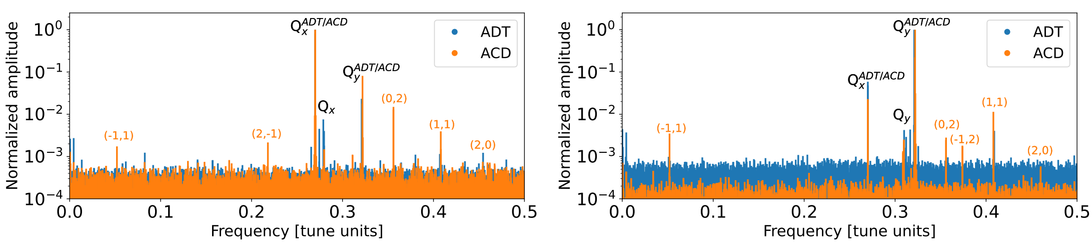

__Figure 5.6.__ Horizontal (left) and vertical (right) frequency spectra of Beam 1 at BPM.10L4.B1 at injection energy for ADT and ac dipole measurements with ADT excitation of 40 000 turns.

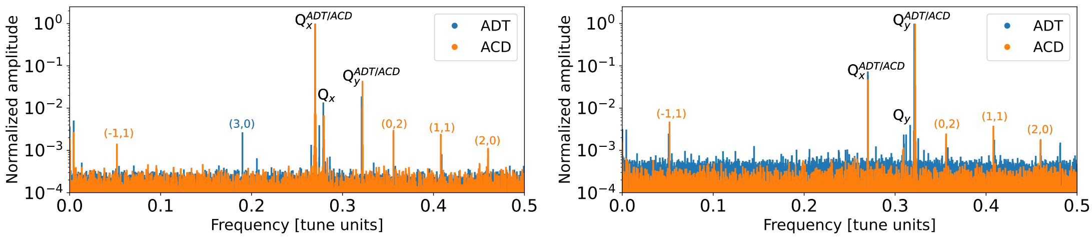

Figure 5.7. *Horizontal (left) and vertical (right) frequency spectra of Beam 2 at BPM.10L4.B2 at injection energy for ADT and ac dipole measurements with ADT excitation of 40 000 turns.*

An increase to the number of turns for ADT measurements provided a significant improvement on the phase resolution, as seen in Fig. 5.8. With 40 000 acquired turns, the phase errors are comparable with a standard optics measurement using the ac dipole, when the ADT measurement action is over 3×10^{-5} m.

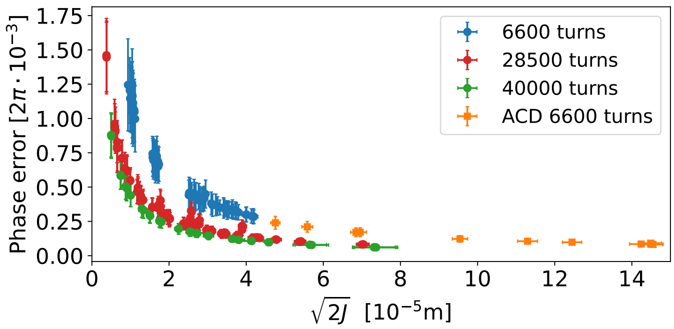

Figure 5.8. *Phase error as a function of oscillation amplitude for ADT and ac dipole (ACD) excitations at injection with different number of turns for ADT.*

As observed from the frequency spectra, increase in the oscillation amplitude and the number of turns improved the signal-to-noise ratio. The signal-to-noise ratio as a function of the action $\sqrt{2J}$ for ADT measurements with different numbers of turns and reference ac dipole measurements at injection is presented in Fig. 5.9.

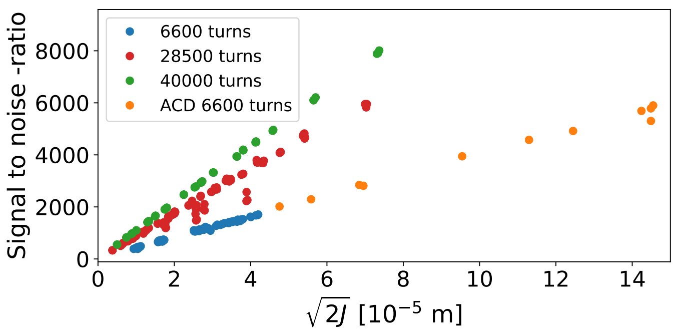

Figure 5.9. *Signal-to-noise ratio as a function of oscillation amplitude for ADT and ac dipole (ACD) excitations at injection with different number of turns for ADT.*

Improvements in the ADT spectral resolution improved the maximum achieved signal-to-noise ratio with a factor of 8 compared to ADT excitations of 6600 turns. With ADT measurements of 40 000 turns, the signal-to-noise ratio is higher than with ac dipole measurements, even though the action is lower.

5.1.2 β-beating at injection

A comparison of the horizontal and vertical β-beating at injection energy for ADT and ac dipole measurements during MD9549 are shown in Figs. 5.10 and 5.11 for Beam 1 and Beam 2, respectively. Optics calculations have been done using OMC3 for multiple measurements with same measurement conditions.

Between the two beam excitation methods, a good agreement can be observed in both planes, with β-beating below 10 % for the majority of the machine. Some deviation can be seen, but the differences in the two methods are within the ac dipole measurement errors, as shown in Fig. 5.12 for the horizontal plane of Beam 1. The comparison of the difference between the β-beating of ADT and ac dipole measurements to the measurement errors of ac dipole gives an outlook on if the discrepancy between the excitation methods is within tolerances, as demonstrated in Fig. 5.12. The graph of the horizontal plane of Beam 1 is representative for both planes of both beams. The results obtained demonstrate that the ADT can reliably be used for optics measurements at injection energy.

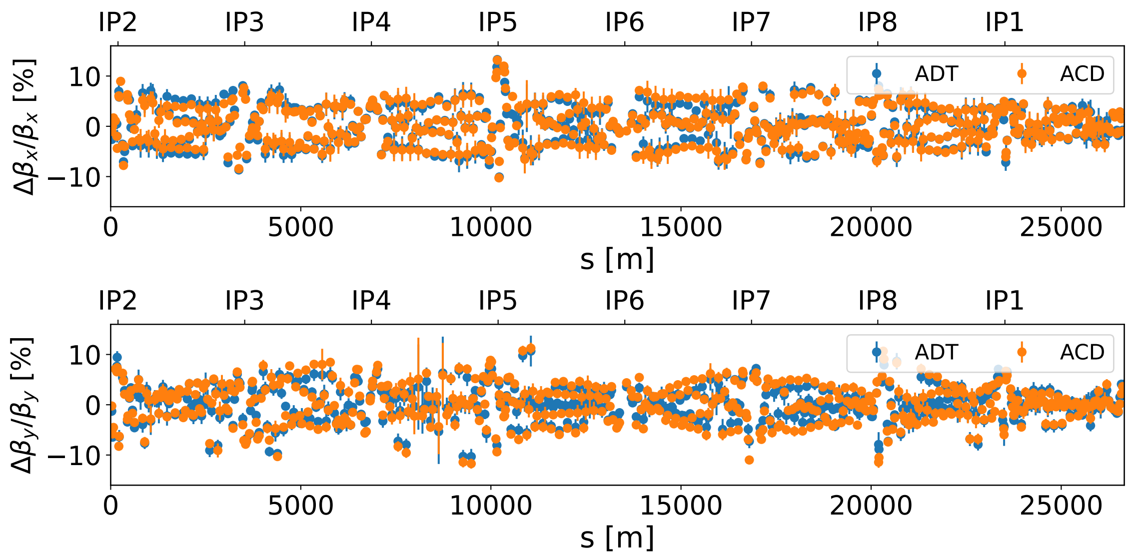

Figure 5.10. *Horizontal (top) and vertical (bottom) β-beating of Beam 1 at injection energy for ADT and ac dipole (ACD) measurements with ADT excitation of 28 500 turns.*

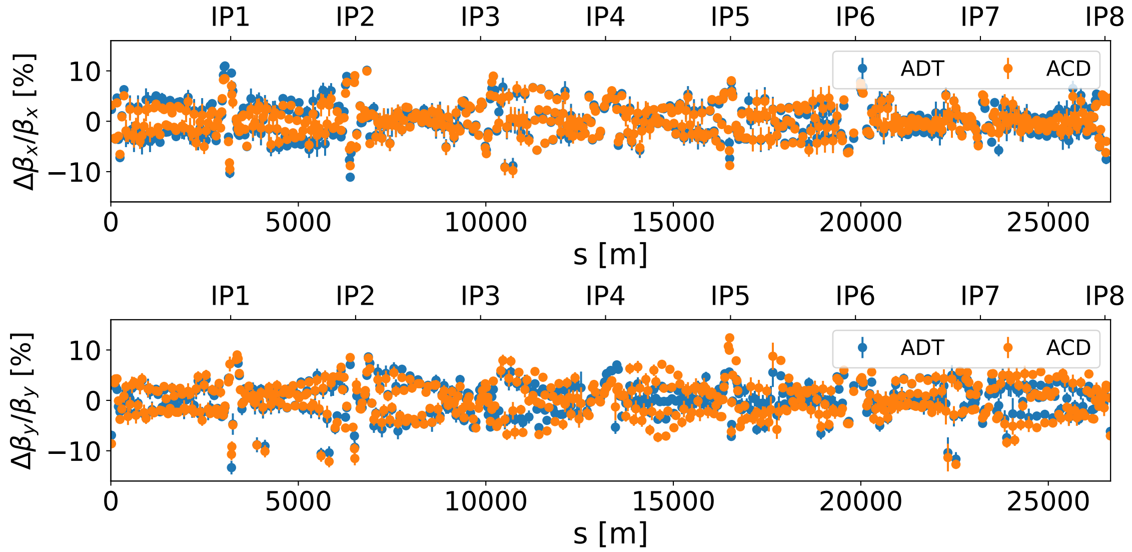

Figure 5.11. *Horizontal (top) and vertical (bottom) β-beating of Beam 2 at injection energy for ADT and ac dipole (ACD) measurements with ADT excitation of 28 500 turns.*

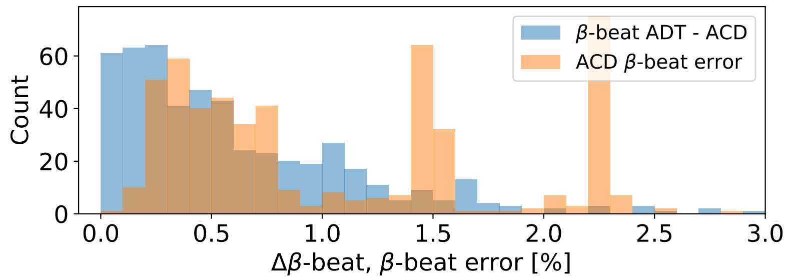

Figure 5.12. *Comparison of error in β-beating for ac dipole measurements and difference in β-beating between the ADT and ac dipole for the horizontal plane of Beam 1 with ADT excitation of 28 500 turns.*

A comparison of β-beating for ADT and ac dipole measurements taken during recommissioning with ADT excitation of 40 000 turns is presented in Figs. 5.13 and 5.14 for Beam 1 and Beam 2, respectively. Optics calculations have been done using OMC3 for multiple measurements. The β-beating is around 5 % for most of the machine and the two excitation methods agree well. As with the previous measurements, the deviation between the ADT and the ac dipole is mostly within the β-beat error of the ac dipole measurement as seen in Fig. 5.15, further confirming that beam excitation with the ADT for optics measurements at injection energy is reliable.

The difference between β-beating in these measurements and measurements during MD9459 arises from different machine conditions and working points. From Table 5.1 it can be seen that the natural tunes and driven tunes differ from each other, as well as the tune split of the vertical plane.

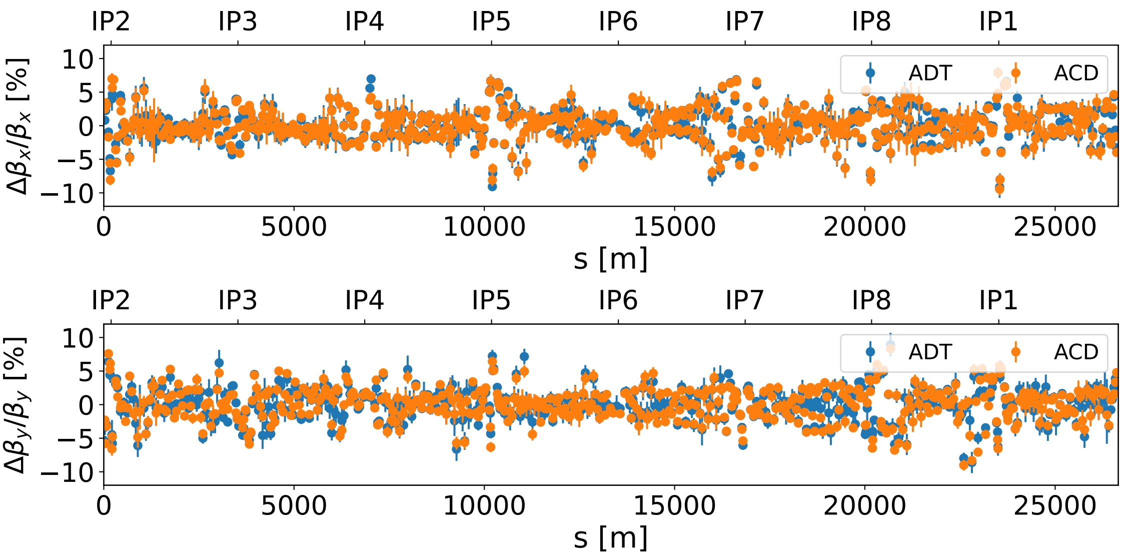

Figure 5.13. *Horizontal (top) and vertical (bottom) β-beating of Beam 1 at injection energy for ADT and ac dipole (ACD) measurements with ADT excitation of 40 000 turns.*

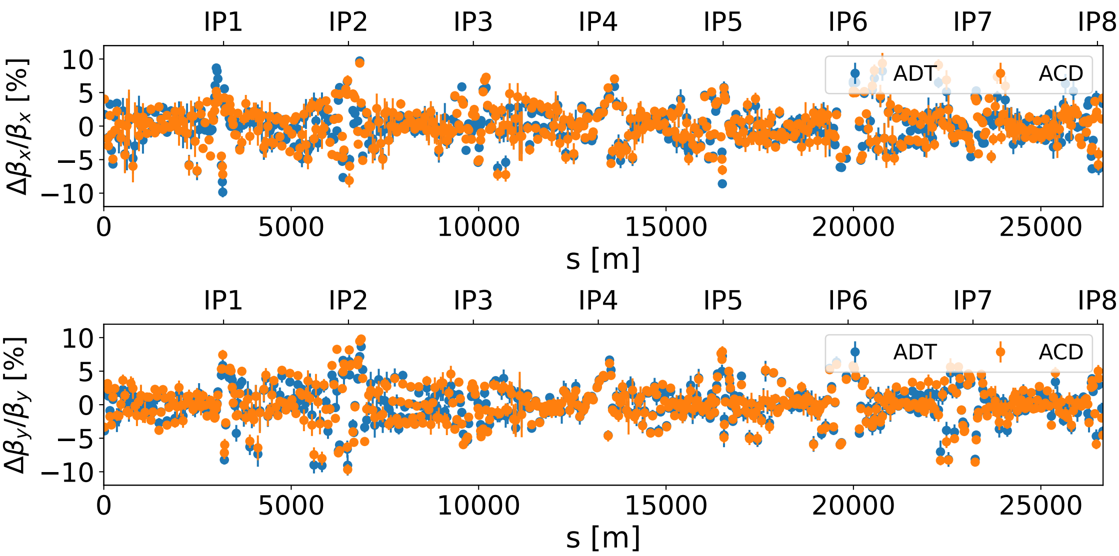

Figure 5.14. *Horizontal (top) and vertical (bottom) β-beating of Beam 2 at injection energy for ADT and ac dipole (ACD) measurements with ADT excitation of 40 000 turns.*

5.2 Linear optics at top energy

During recommissioning on August 31, 2023, ADT measurements were taken at top energy with $\beta^*_{\mathrm{IP1,IP5}} = 30\ \mathrm{cm}$ with data acquisition of 40 000 turns to further validate the use of the ADT for optics measurements towards operational conditions. The measurements were performed using single pilot bunches, and the natural and driven tunes were $Q_x = 0.280$ and $Q_x^{\mathrm{ADT}} = 0.270$ for the horizontal plane and $Q_y = 0.310$ and $Q_y^{\mathrm{ADT}} = 0.325$ for the vertical plane. The horizontal and vertical frequency spectra for a single ADT measurement are compared to an ac dipole measurement in Figs. 5.16 and 5.17 for Beam 1 and Beam 2, respectively. The noise floor for both excitation methods

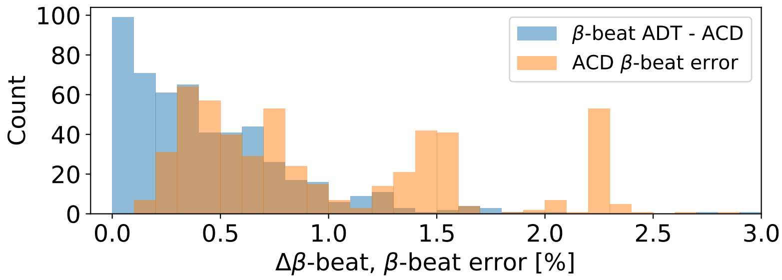

Figure 5.15. *Comparison of error in β-beating for ac dipole measurements and difference in β-beating between the ADT and ac dipole for the horizontal plane of Beam 1 with ADT excitation of 40 000 turns.*

is higher than with measurements at injection due to stricter machine conditions at top energy. Figures 5.16 and 5.17 indicate that the noise floor with ADT measurements is higher than ac dipole measurements for both beams and both planes, indicating the need for a stronger oscillation for ADT to obtain a comparable spectral resolution. The set kick amplitude from the measurement software was the same as with measurements at injection, but the actions are much lower, as seen in Table 5.1.

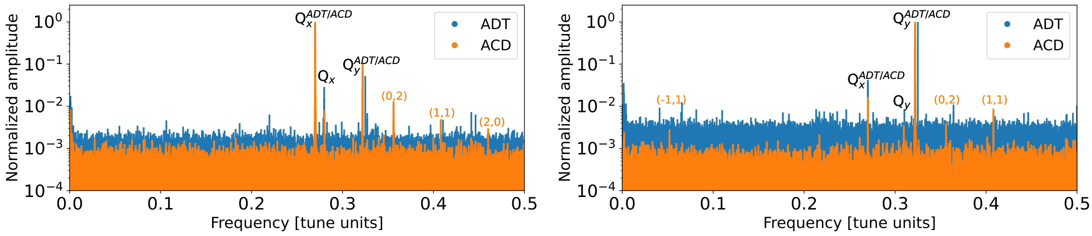

Figure 5.16. *Horizontal (left) and vertical (right) frequency spectra of Beam 1 at BPM.10L5.B1 at top energy with $\beta^*_{\mathrm{IP1,IP5}} = 30\ \mathrm{cm}$ for ADT and ac dipole measurements with ADT excitation of 40 000 turns.*

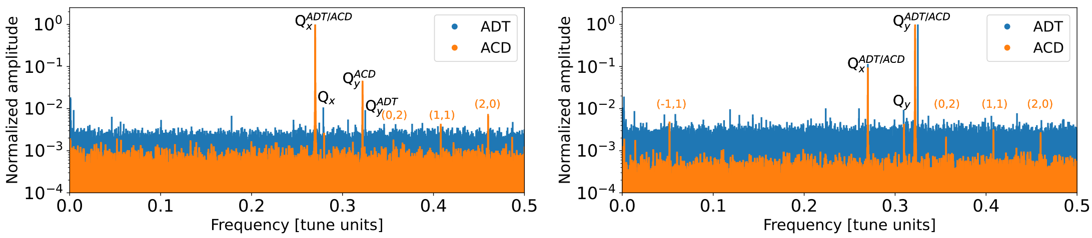

Figure 5.17. *Horizontal (left) and vertical (right) frequency spectra of Beam 2 at BPM.10L5.B2 at top energy with $\beta^*_{\mathrm{IP1,IP5}} = 30\ \mathrm{cm}$ at top energy for ADT and ac dipole measurements with ADT excitation of 40 000 turns.*

A comparison of β-beating for ADT and ac dipole measurements taken with $\beta^*_{\mathrm{IP1,IP5}} = 30\ \mathrm{cm}$ is shown in Figs. 5.18 and 5.19 for Beam 1 and Beam 2 respectively, with several measurements analysed together using OMC3. At top energy, the measured β-beating with the ADT is higher than with the ac dipole with peak β-beating of over 10 %, relating to an insufficient excitation amplitude. In order to improve the measurement quality with ADT measurements, the tune split could be reduced to allow for a stronger excitation.

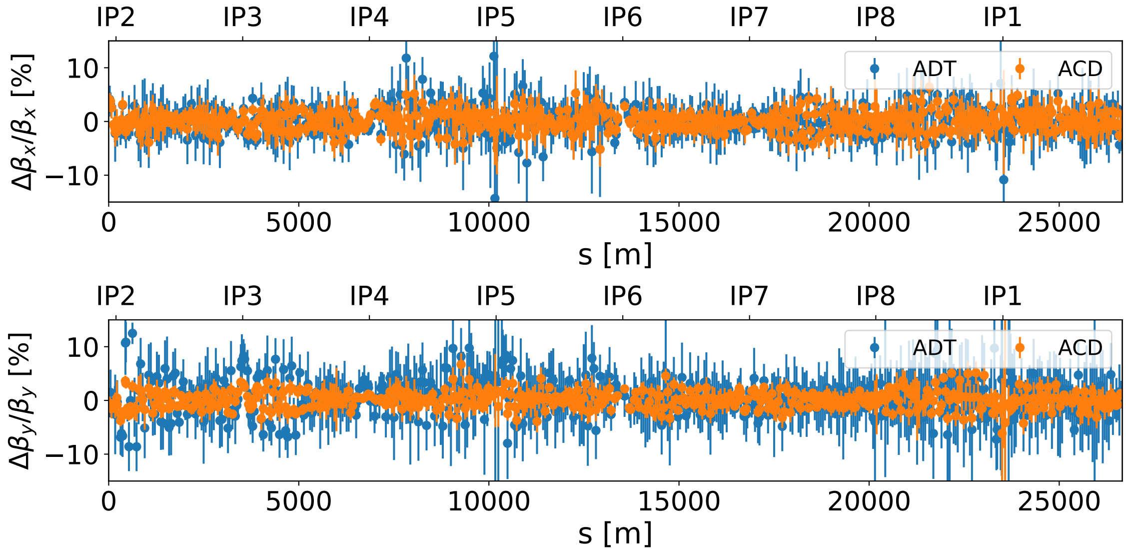

Figure 5.18. *Horizontal (top) and vertical (bottom) β-beating of Beam 1 at top energy with $\beta^*_{\mathrm{IP1,IP5}} = 30$ cm for ADT and ac dipole (ACD) measurements.*

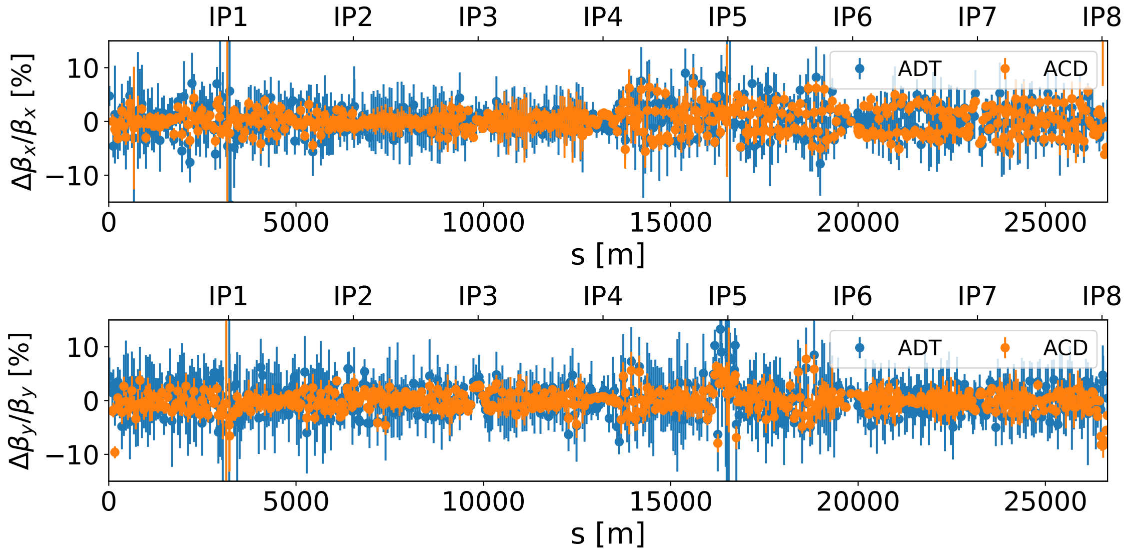

Figure 5.19. *Horizontal (top) and vertical (bottom) β-beating of Beam 2 at top energy with $\beta^*_{\mathrm{IP1,IP5}} = 30$ cm for ADT and ac dipole (ACD) measurements.*

The difference between the β-beating of the ADT and the ac dipole is larger than the β-beat errors of the ac dipole, as seen in Fig. 5.20 for Beam 1. For the horizontal plane of Beam 1, the quality of the measurement is within the ac dipole β-beating error tolerances, but in the vertical plane, the difference is larger. In order to improve the ADT measurement quality to a comparable level with the ac dipole, a higher amplitude for the ADT would be necessary.

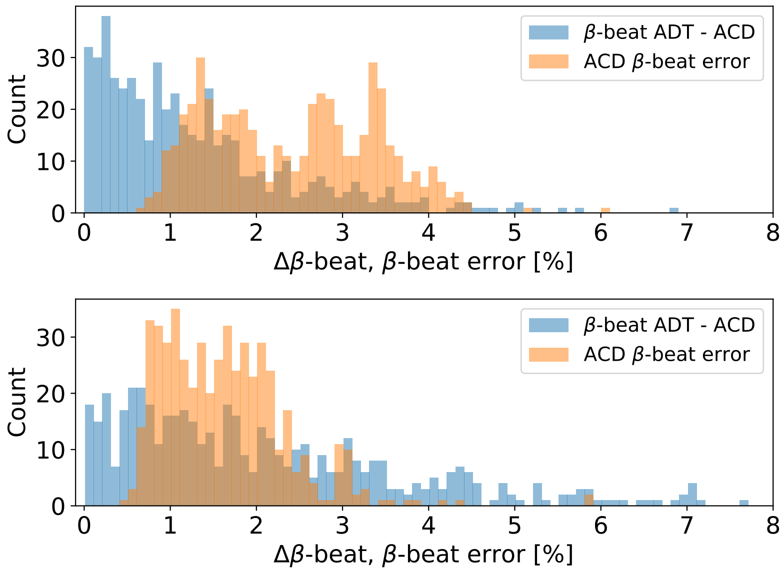

Figure 5.20. *Comparison of error in β-beating for ac dipole measurements and difference in β-beating between the ADT and ac dipole for the horizontal (top) and vertical (bottom) plane of Beam 1 at top energy with $\beta^*_{\mathrm{IP1,IP5}} = 30\ \mathrm{cm}$.*

At top energy, ADT measurements were taken on June 8, 2023 during commissioning for the high-β^* run with $\beta^* = 120\ \mathrm{m}$ at IP1 and IP5. Instead of squeezing the beam size at the IPs for maximum luminosity, the beam is de-squeezed to have a low beam divergence needed for research of elastic proton scattering in the TOTEM [57] and ATLAS/ALFA [58] experiments. The frequency spectra of a single ADT measurement compared to a single ac dipole measurement for both beams are shown in Figs. 5.21 and 5.22 using the highest possible set amplitude from the ADT acquisition software and 40 000 turns at flat top. The natural and driven tunes used for these measurements were $Q_x = 0.280$ and $Q_x^{\mathrm{ADT}} = 0.270$ for the horizontal plane and $Q_y = 0.310$ and $Q_y^{\mathrm{ADT}} = 0.320$ for the vertical plane. The noise floor of both the ADT and the ac dipole measurements is again higher than at injection, and the noise floor of ac dipole measurements is lower than with the ADT. The measured actions of the ADT acquisitions in Table 5.1 are low at around 1×10^{-5} m, contributing to a higher noise floor on the frequency spectrum.

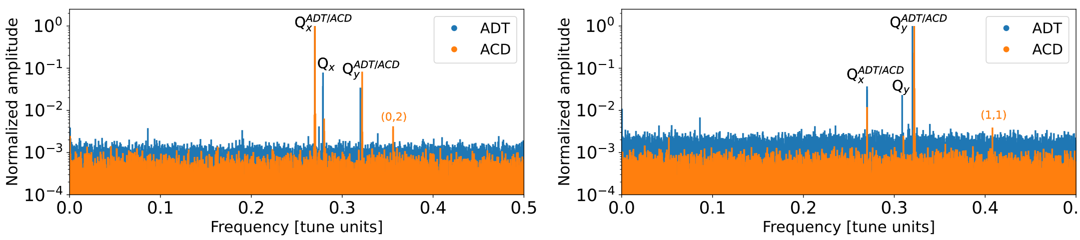

Figure 5.21. *Horizontal (left) and vertical (right) frequency spectra of Beam 1 at top energy with $\beta^*_{\mathrm{IP1,IP5}} = 120\ \mathrm{m}$ at BPM.10L5.B1 for ADT and ac dipole measurements with ADT excitation of 40 000 turns.*

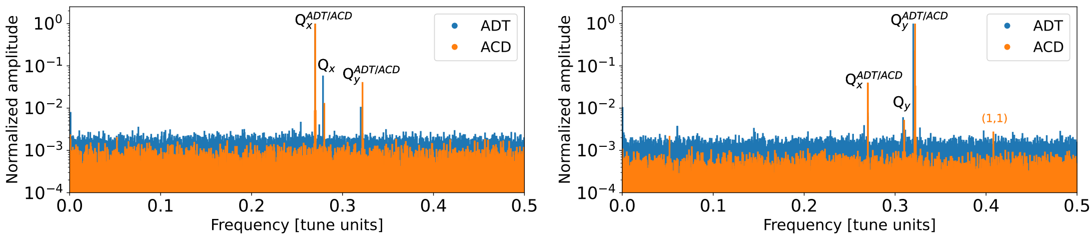

Figure 5.22. *Horizontal (left) and vertical (right) frequency spectra of Beam 2 at top energy with* $\beta^*_{\mathrm{IP1,IP5}} = 120\ \mathrm{m}$ *at BPM.10L5.B2 for ADT and ac dipole measurements with ADT excitation of 40 000 turns.*

A comparison of β-beating between ADT and ac dipole high-β measurements for Beam 1 and Beam 2 is presented in respective Figs. 5.23 and 5.24, with optics calculations performed using OMC3 for multiple measurements. Some agreement is observed between the two excitation methods, although not as strong as with measurements at injection. The β-beating is less than 10 % for the entire machine, and in most sections below 5 %. The difference between the two excitation methods is larger than what would be tolerable for the ac dipole measurement error tolerances, as seen in Fig. 5.25 for the horizontal plane of Beam 1, representing the conditions with both beams and planes.

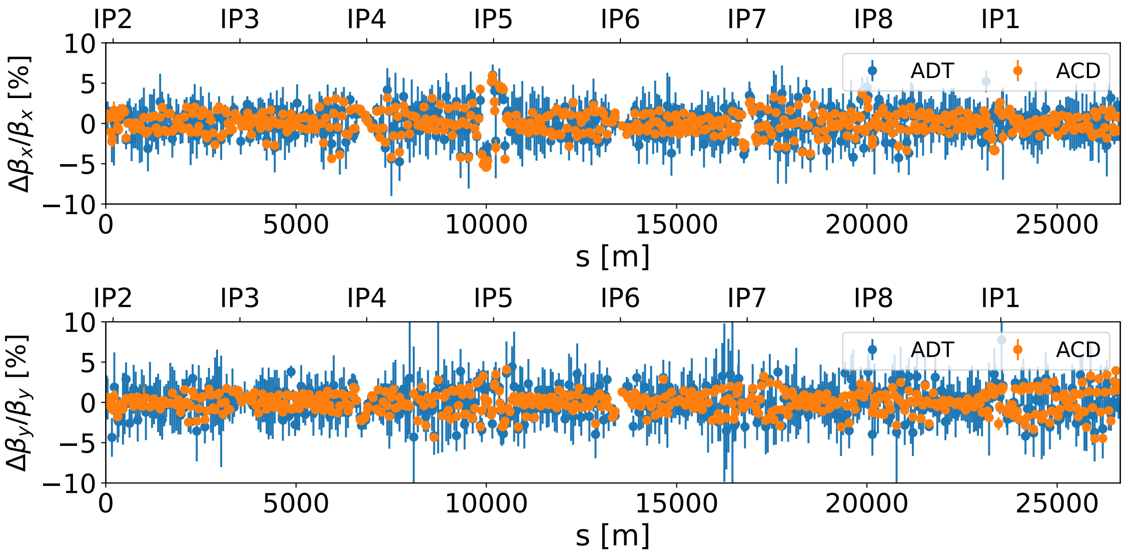

Figure 5.23. *Horizontal (top) and vertical (bottom)* β*-beating of Beam 1 at top energy with* $\beta^*_{\mathrm{IP1,IP5}} = 120\ \mathrm{m}$ *for ADT and ac dipole measurements.*

ADT measurements at top energy performed in these studies provide a base for improving the spectral quality. The increased number of turns did not improve the measurement quality to a comparable level with reference ac dipole measurements. Future studies should consider reducing the tune split for increasing the oscillation amplitude by exciting closer to the natural tune.

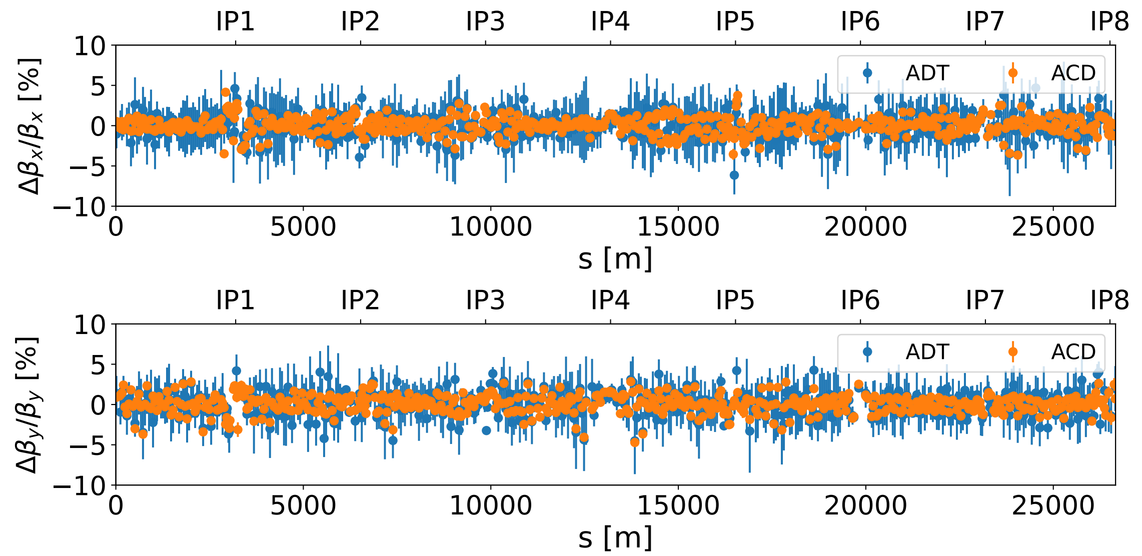

Figure 5.24. *Horizontal (top) and vertical (bottom) β-beating of Beam 2 at top energy with $\beta^*_{\mathrm{IP1,IP5}} = 120\ \mathrm{m}$ for ADT and ac dipole measurements.*

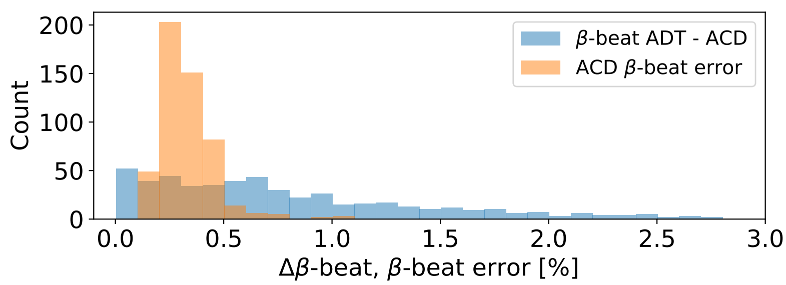

Figure 5.25. *Comparison of error in β-beating for ac dipole measurements and difference in β-beating between the ADT and ac dipole for the horizontal plane of Beam 1 at top energy with $\beta^*_{\mathrm{IP1,IP5}} = 120\ \mathrm{m}$.*

5.3 Measurements in the ramp of the ion cycle

Part of the 2023 run of the LHC was dedicated to heavy-ion physics measurements, using lead ions instead of protons. The operational cycle is different compared to operation with protons, and separate optics commissioning needs to be performed. The 2023 ion run was challenging, and several issues arose [59]. Among those, transverse beam losses were observed during ramp at around 6.3 TeV causing beam dumps and limiting the total intensity, resulting in downtime.

Measurements with the ion cycle during the simultaneous ramp and squeeze were performed using the ADT to check the change in β-beating during the ramp. ADT measurements were done with 6600 turns and using a single pilot bunch with the ion cycle setup but using protons. Corresponding ac dipole measurements during the ramp were performed with the same optics configuration, but using lead ions instead of protons. Figure 5.26 shows a comparison of RMS β-beating over all BPMs during the ramp for

Beam 1 and Beam 2 between ADT and ac dipole measurements.

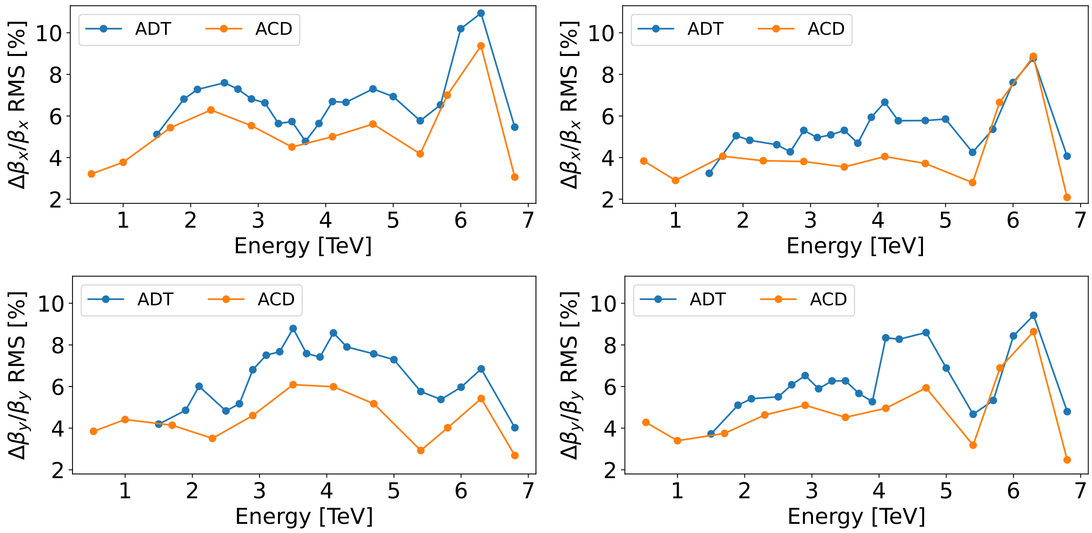

Figure 5.26. *Comparison of horizontal and vertical β-beat RMS over all BPMs during ramp with the ion cycle for Beam 1 (left) and Beam 2 (right) for ADT and ac dipole measurements.*

The fast reloading of the ADT permits for more measurements during the ramp with the ac dipole, giving more data on the optics behaviour. The same behaviour of the RMS β-beating during the ramp is observed with both excitation methods. An increase in β-beat RMS is observed at around 6.3 TeV and decrease again at 6.8 TeV for both beams. For the vertical plane of Beam 1, β-beat RMS reaches its maximum values at energies between 3 and 4.5 TeV instead of 6.3 TeV, but an increase in the RMS β-beating at 6.3 TeV can be observed as with the other plane and beam. With the ac dipole, the kick strength increases during the ramp to keep the action approximately consistent during the measurements. ADT measurements have the same set amplitude from the software, resulting in a decreasing kick amplitude during the ramp and possibly affecting the measurement quality.

In general, measurements with both the ac dipole and the ADT show a decrease in optics control at 6.3 TeV that contributes to losses in the ramp. The source of the transverse beam losses is still not fully understood, and possible causes to the increase in β-beating include an energy mismatch of the triplet magnets close to the IPs [60]. While the number of turns acquired for the ADT excitation was not ideal for good quality optics measurements, it can still be used to identify optics deviations in operation.

5.4 Observation of resonance driving terms with the ADT

Increase in the duration of acquired turn-by-turn data and a higher kick amplitude increased the spectral resolution, revealing secondary spectral lines in the frequency spectrum of ADT excitations at injection energy. Figure 5.27 shows the horizontal frequency spectrum for an ADT excitation with 28 500 turns of Beam 2 during MD9549. Analysis of the secondary spectral lines in this thesis is performed only for Beam 2 due to the larger oscillation amplitude and stronger observation of the secondary modes.

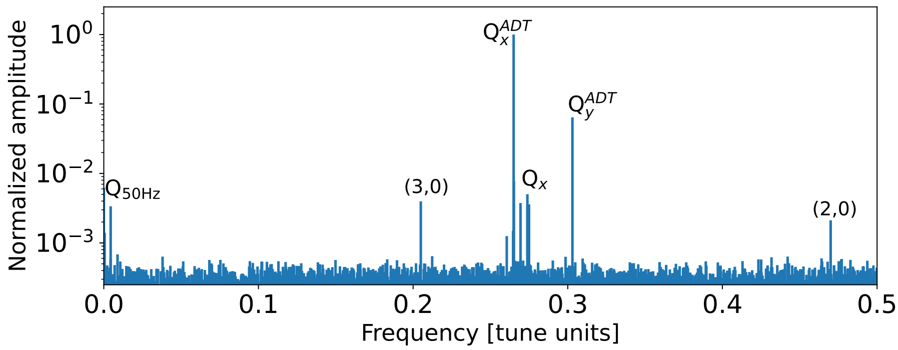

Figure 5.27. *Horizontal frequency spectrum of an ADT measurement of Beam 2 at injection energy during MD9549 with ADT excitation of 28 500 turns.*

The spectral line $(2, 0)$ at the frequency $2Q_x^{\mathrm{ADT}}$ corresponds to two resonance driving terms of a normal sextupole, $f_{1200,H}$ and $f_{3000,H}$, and the line $(3, 0)$ at the frequency $3Q_x^{\mathrm{ADT}}$ corresponds to the normal octupolar resonance driving terms $f_{1300,H}$ and $f_{4000,H}$. As resonance driving terms have not been measured with the ADT before, the analysis conducted in this thesis focuses on the lowest order multipole. The resonance driving terms were calculated using the OMC3 software. The calculated sextupolar driving terms $f_{1200,H}$ and $f_{3000,H}$ for ADT and ac dipole measurements are presented respectively in Figs. 5.28 and 5.29 with 28 500 turns of ADT acquisition. The horizontal natural tune was $Q_x = 0.275$, and the driven tune was $Q_x^{\mathrm{ADT}} = 0.265$.

Some qualitative agreement can be observed of the amplitudes of the resonance driving terms $f_{1200,H}$ and $f_{3000,H}$ between the two excitation methods as seen in Figs. 5.28 and 5.29. The amplitude of the RDTs is of same magnitude, but measurements with the ADT lose the amplitude variations of the RDT, as seen with the ac dipole. This may be due to the small oscillation amplitude in combination with the current data cleaning methods. The phases of the RDTs between the ADT and ac dipole show some variance.

Figures 5.30 and 5.31 show the real and imaginary parts of $f_{1200,H}$ and $f_{3000,H}$ of ADT and ac dipole measurements. The large outliers at the vicinity of the IPs are due to the phase differences of 0 or π, making the momentum coordinate reconstruction complex. The amplitude of the real and imaginary terms of ADT is smaller than of the ac dipole throughout the machine for $f_{1200,H}$, while the $f_{3000,H}$ terms have a better agreement.

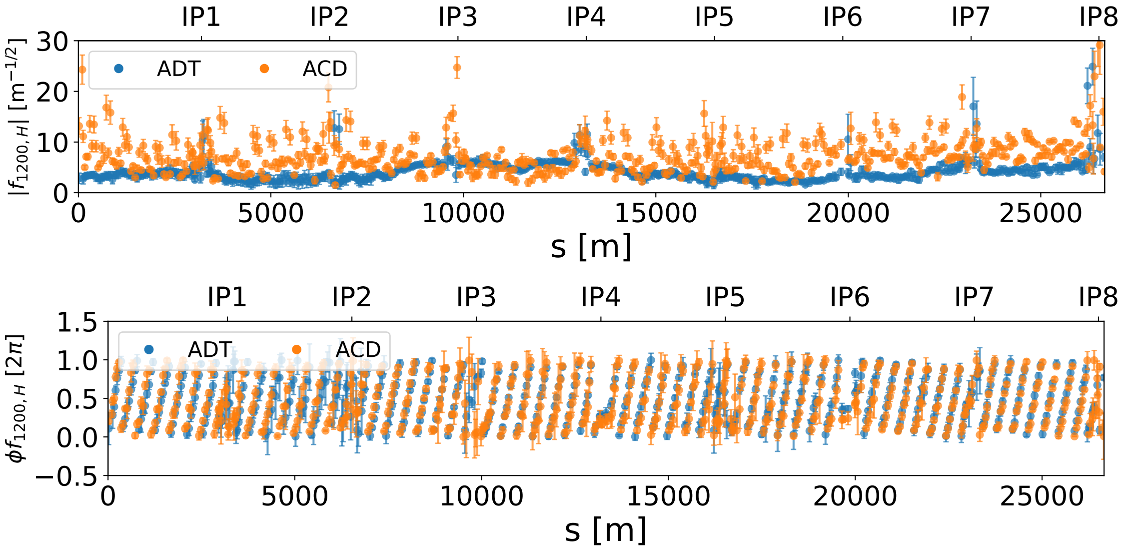

Figure 5.28. *Amplitude (top) and phase (bottom) comparison of the normal sextupolar resonance driving term $f_{1200,H}$ of Beam 2 for ADT and ac dipole measurements at injection energy during MD9549.*

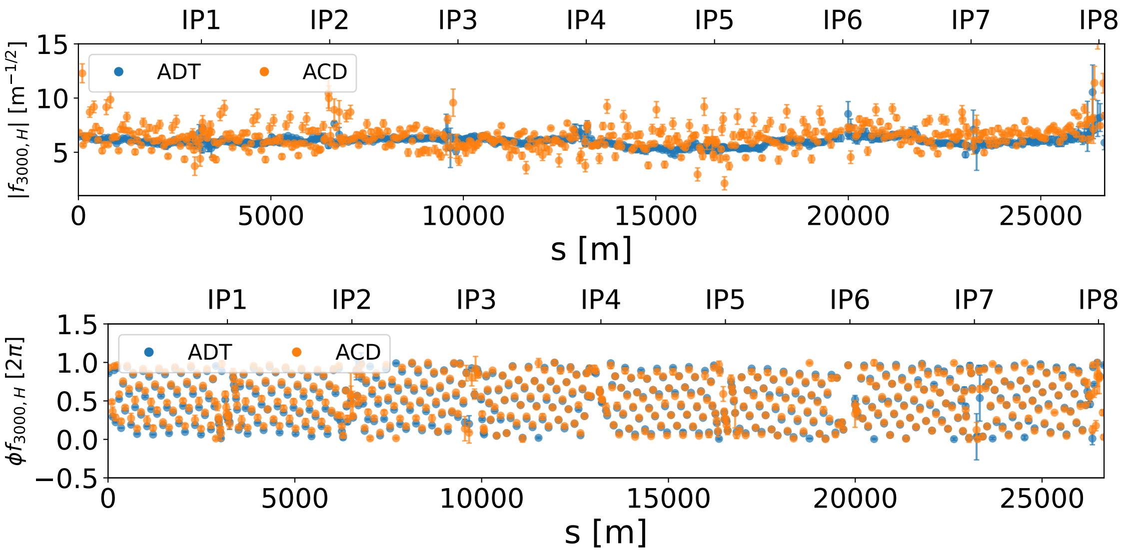

Figure 5.29. *Amplitude (top) and phase (bottom) comparison of the normal sextupolar resonance driving term $f_{3000,H}$ of Beam 2 for ADT and ac dipole measurements at injection energy during MD9549.*

Measurements during the recommissioning after the triplet repair were performed with a different working point and with more turns than MD9549. The vertical frequency spectra of Beam 2 of an ADT excitation during recommissioning with 40 000 turns is shown in Fig. 5.32. In addition to the spectral lines $(2, 0)$ and $(3, 0)$ observed during MD9549, the line $(1, 1)$ was visible in the frequency spectrum of recommissioning ADT measurements corresponding to resonance driving terms $f_{0111,V}$ and $f_{1020,V}$.

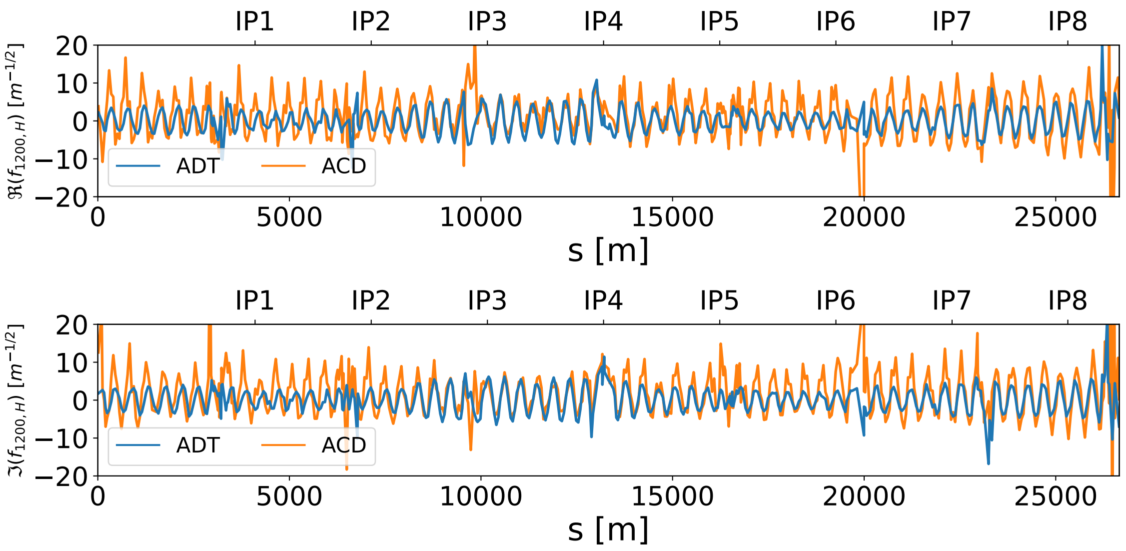

Figure 5.30. *Comparison of the real (top) and imaginary (bottom) part of the resonance driving term $f_{1200,H}$ of Beam 2 for ADT and ac dipole measurements at injection energy during MD9549.*

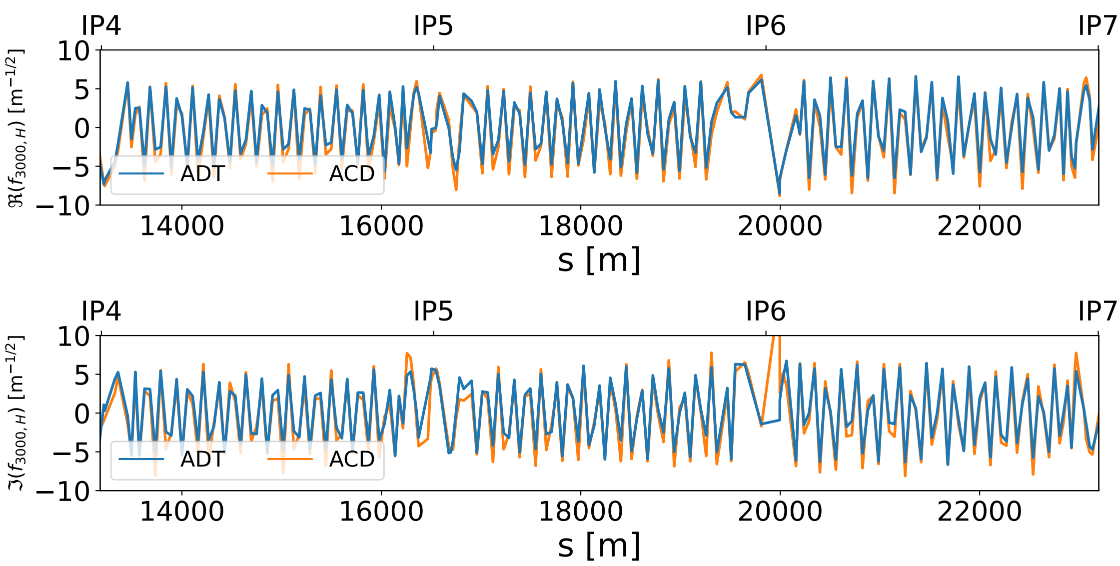

Figure 5.31. *Comparison of the real (top) and imaginary (bottom) part of the resonance driving term $f_{3000,H}$ of Beam 2 for ADT and ac dipole measurements at injection energy during MD9549. The data shown is a representative sample of the whole machine.*

The calculated sextupolar driving terms $f_{1200,H}$ and $f_{3000,H}$ corresponding to the line $(2,0)$ and the frequency $2Q_x^{\mathrm{ADT}}$ for ADT and ac dipole measurements during recommissioning are presented in Figs. 5.33 and 5.34.

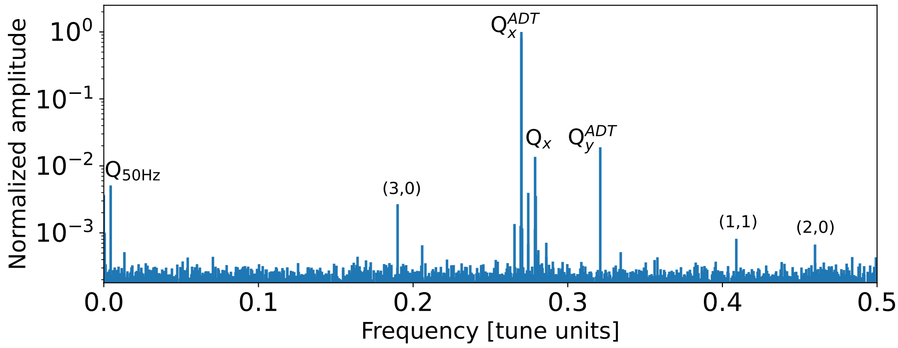

Figure 5.32. *Horizontal frequency spectrum of an ADT measurement of Beam 2 at injection energy during recommissioning with ADT excitation of 40 000 turns.*

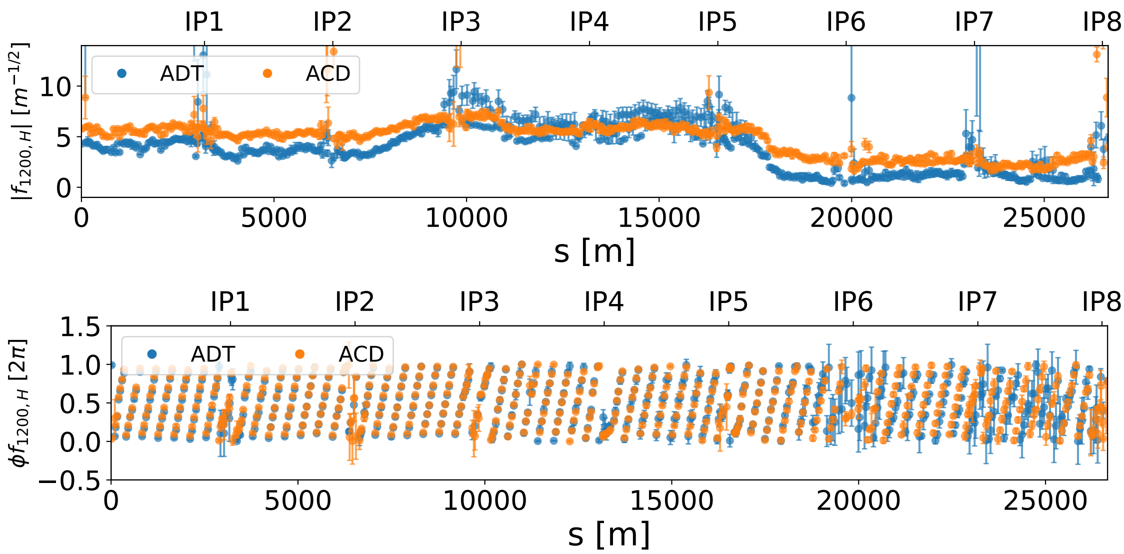

Figure 5.33. *Amplitude (top) and phase (bottom) comparison of the normal sextupolar resonance driving term* $f_{1200,H}$ *of Beam 2 for ADT and ac dipole measurements at injection energy during recommissioning.*

The amplitude and the phase of the resonance driving terms $f_{1200,H}$ and $f_{3000,H}$ have a better agreement between the ADT and the ac dipole when compared to measurements during MD9549. It can be seen from Fig. 5.33 that the $f_{1200,H}$ RDT increases from IP2 to IP3, and again decreases from IP5 to IP6, and this behaviour can be seen with both excitation methods. For the $f_{3000,H}$ term in Fig. 5.34, both excitation methods show the amplitude of the RDT decreasing from IP3 and increasing again on IP5, although the pattern is less clear than with $f_{1200,H}$. Changes in the RDT in specific locations may indicate a source in the area causing the change, and need to be investigated in more detail.

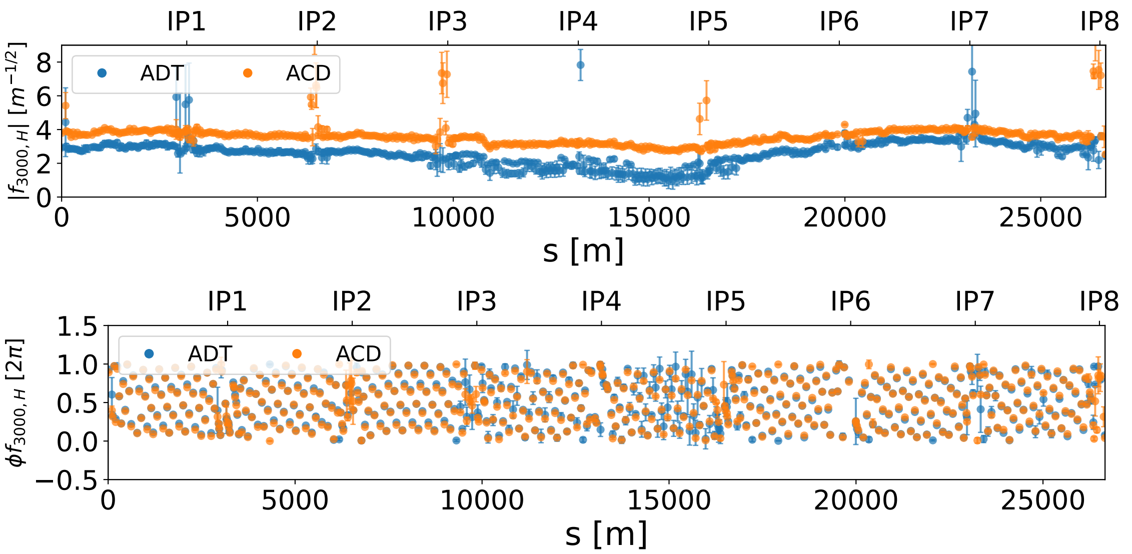

Figure 5.34. *Amplitude (top) and phase (bottom) comparison of the normal sextupolar resonance driving term $f_{3000,H}$ of Beam 2 for ADT and ac dipole measurements at injection energy during recommissioning.*

The real and imaginary terms of the $f_{1200,H}$ and $f_{3000,H}$ RDTs are shown in respective Figs. 5.35 and 5.36. The agreement between the two excitation methods is better than with MD9549 measurements. In some arcs the amplitudes of the real and imaginary terms with the ADT are smaller than with the ac dipole, matching the difference of amplitudes in Figs. 5.33 and 5.34.

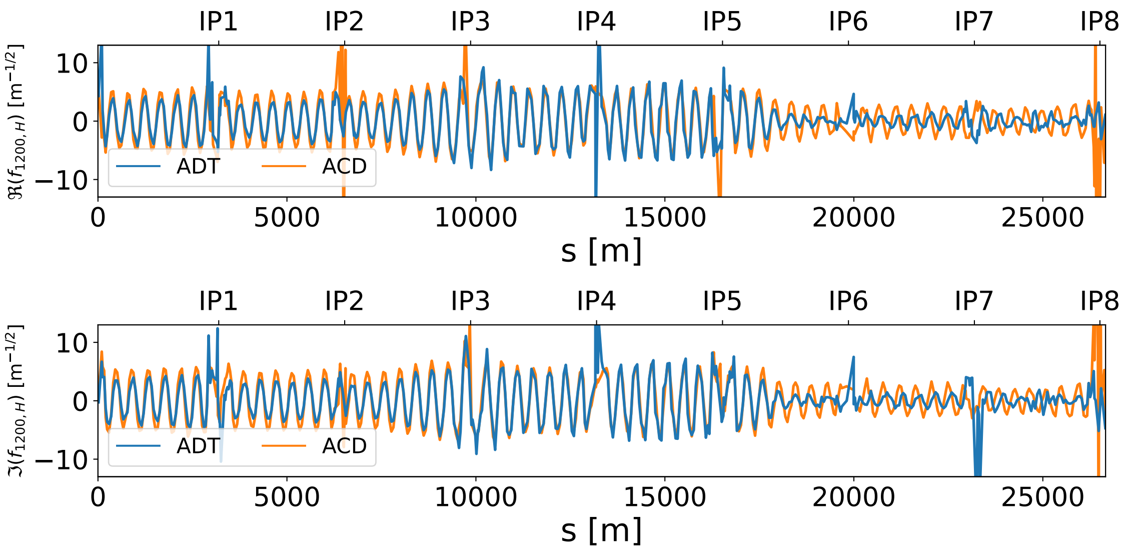

Figure 5.35. *Comparison of the real (top) and imaginary (bottom) part of the resonance driving terms $f_{1200,H}$ of Beam 2 for ADT and ac dipole measurements at injection energy during recommissioning.*

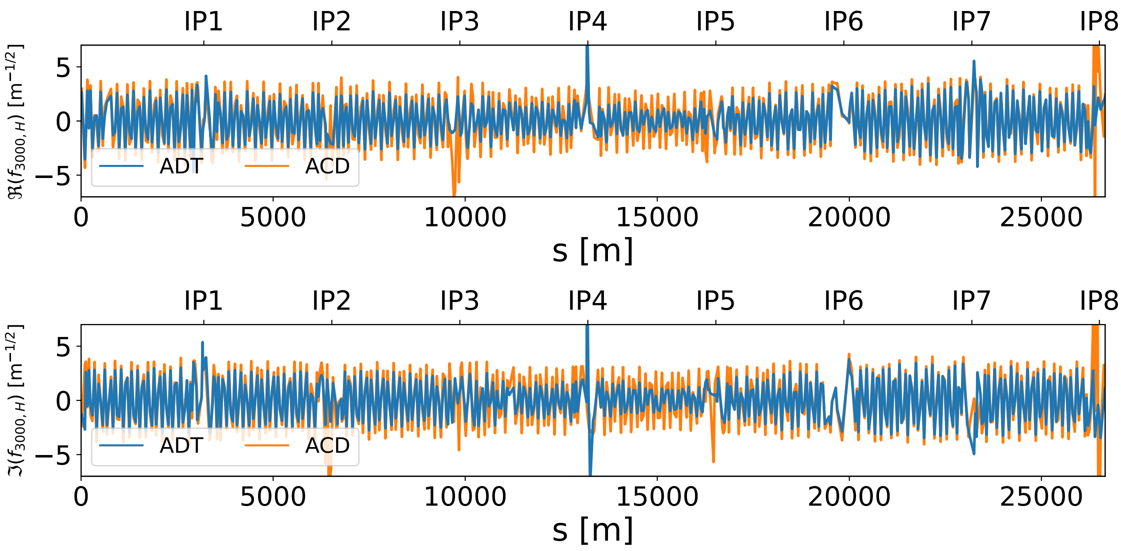

Figure 5.36. *Comparison of the real (top) and imaginary (bottom) part of the resonance driving term $f_{3000,H}$ of Beam 2 for ADT and ac dipole measurements at injection energy during recommissioning.*

In addition, normal sextupolar resonance driving terms $f_{0111,V}$ and $f_{1020,V}$ were calculated for ADT and ac dipole recommissioning measurements. These RDTs correspond to the $(1,1)$ line and the frequency $Q_x^{\mathrm{ADT}} + Q_y^{\mathrm{ADT}}$ in the frequency spectrum in Fig. 5.32. Figures 5.37 and 5.38 show the amplitudes and phases of the RDTs $f_{0111,V}$ and $f_{1020,V}$, and an excellent agreement can be observed between the two excitation methods for both terms. For the $f_{0111,V}$ term, the amplitude of the RDT seems to decrease from IP5, and the same behaviour can be observed with both the ac dipole and the ADT.

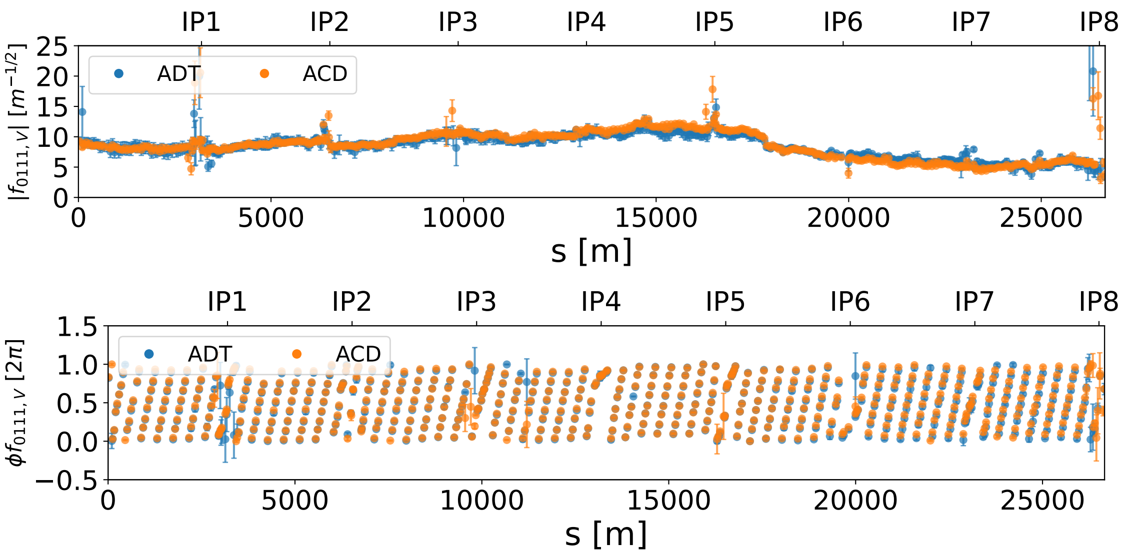

Figure 5.37. *Amplitude (top) and phase (bottom) comparison of the normal sextupolar resonance driving term $f_{0111,V}$ of Beam 2 for ADT and ac dipole measurements at injection energy during recommissioning.*

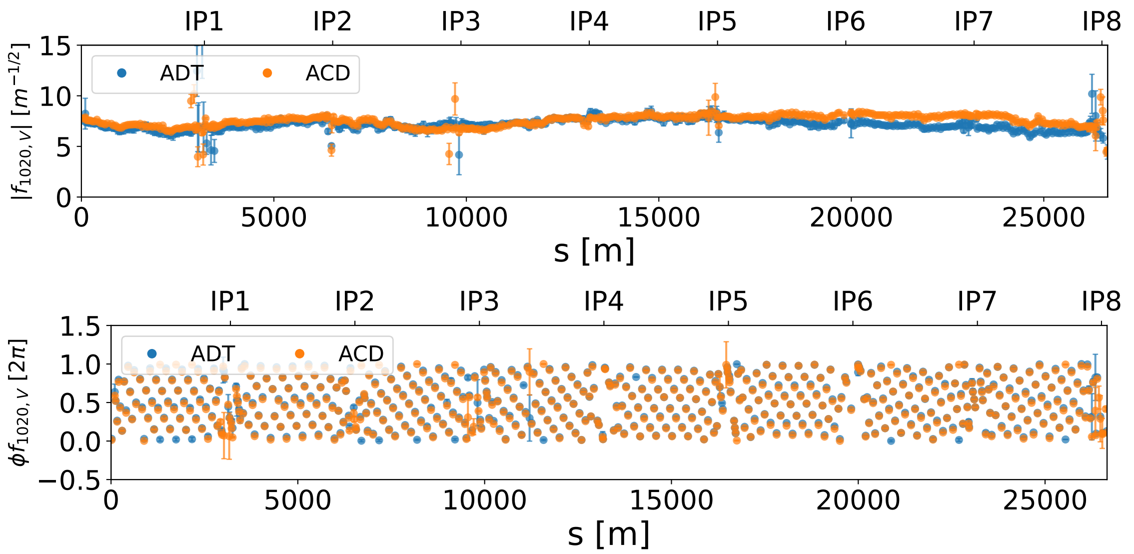

Figure 5.38. *Amplitude (top) and phase (bottom) comparison of the normal sextupolar resonance driving terms $f_{1020,V}$ of Beam 2 for ADT and ac dipole measurements at injection energy during recommissioning.*

The real and imaginary terms of the RDTs $f_{0111,V}$ and $f_{1020,V}$ for ADT and ac dipole measurements are shown in Figs. 5.39 and 5.40. For the $f_{0111,V}$ RDT, the real and imaginary terms have a great agreement, as observed in Fig. 5.39. Some variance is observed with the $f_{1020,V}$ RDT real and imaginary terms in Fig. 5.40, as the amplitude of the RDT is lower between IP6 and IP8, as seen in Fig. 5.38.

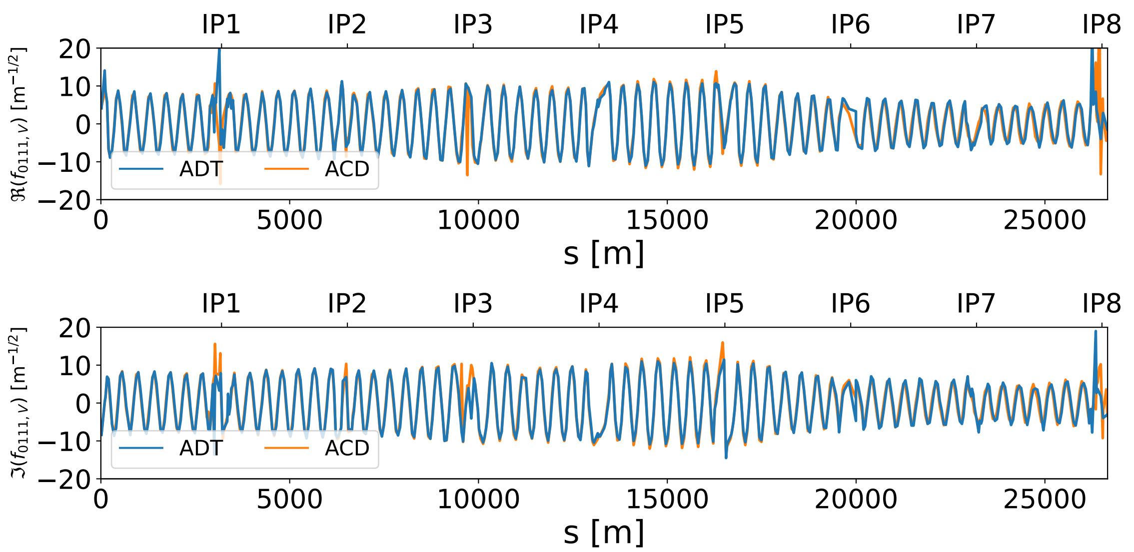

Figure 5.39. *Comparison of the real (top) and imaginary (bottom) part of the resonance driving terms $f_{0111,V}$ of Beam 2 for ADT and ac dipole measurements at injection energy during recommissioning.*

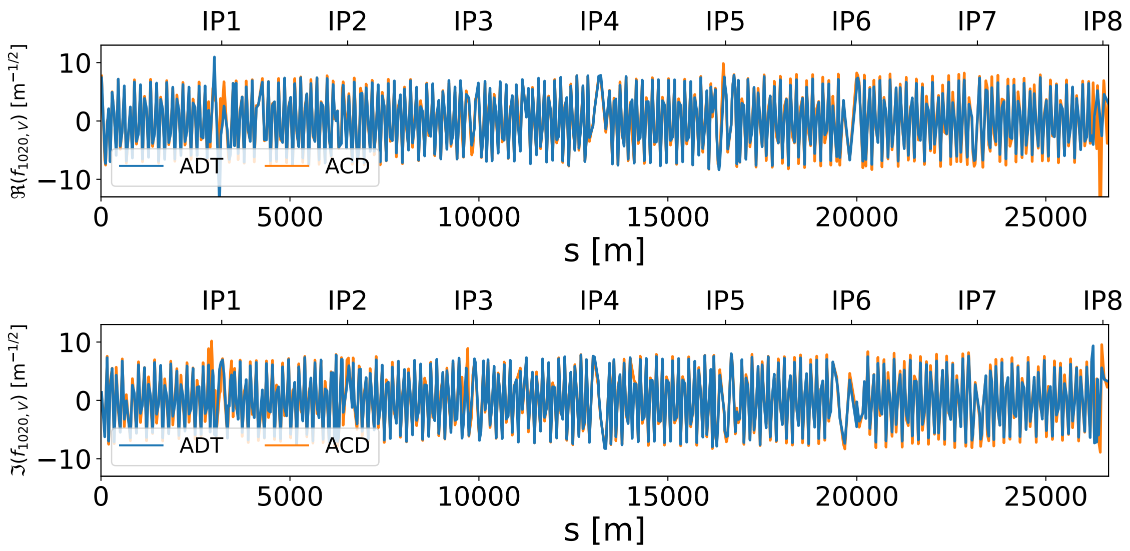

Figure 5.40. *Comparison of the real (top) and imaginary (bottom) part of the resonance driving term $f_{1020,V}$ of Beam 2 for ADT and ac dipole measurements at injection energy during recommissioning.*

Resonance driving terms have not been measured with the ADT before, and the research conducted in this thesis opens the possibility for low-amplitude nonlinear optics measurements with the ADT in the future. Low-amplitude nonlinear optics measurements may allow for studies on the influence of collective effects on nonlinearities.

5.5 Amplitude detuning

Measurements at injection energy during MD9549 with 28 500 turns of ADT excitation included data with increasing oscillation amplitudes to check for possible amplitude detuning. Typically when measuring amplitude detuning with the ac dipole, measurements are performed by increasing the excitation amplitude of a single plane while exciting the other plane with a lower, constant amplitude that is sufficient for measuring the natural tune [39]. With the ADT, the current measurement software sets the excitation amplitude to be the same for both planes, and these diagonal kicks require the amplitude detuning to be analysed as the sum of the horizontal and vertical actions. Figure 5.41 shows the measured natural tune shift as a function of the sum of the horizontal and vertical actions, $2J_x + 2J_y$.

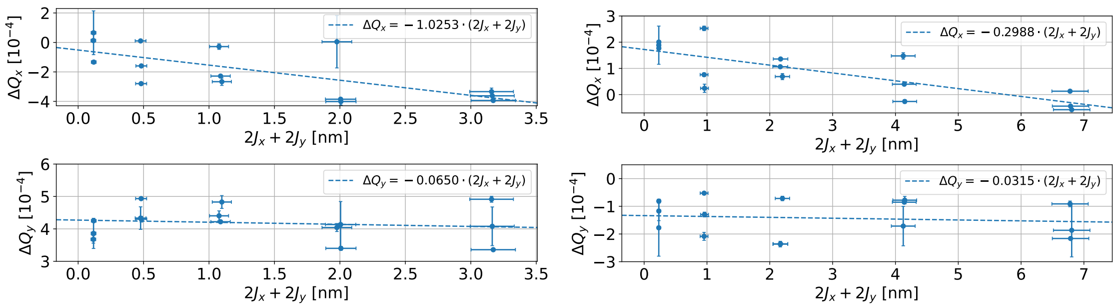

Figure 5.41. *Natural tune shift as a function of sum of horizontal and vertical actions of Beam 1 (left) and Beam 2 (right) for ADT measurements during MD9459.*

Because the oscillation amplitude of the ADT is low, any major change in the natural tune is not visible in measurements, as seen in Fig. 5.41. The horizontal tune appears to go down, but the error bars on the measurements are too strong to conclude. The vertical tune does not seem to change. In order to see amplitude detuning with the ADT, the tune split between the natural tune and driven tune should be set smaller for achieving higher actions. For these measurements, the tune split was $\Delta Q_x = -0.010$ and $\Delta Q_y = +0.010$. Additionally, increasing the oscillation amplitude would benefit the observation of amplitude detuning.

5.6 50 Hz sidebands

The spectral analysis of ADT measurements revealed sidebands around the main mode caused by 50 Hz perturbations. The observation of sidebands in frequency spectrum of transverse beam excitations is new, since they have not been observed with the ac dipole. Such perturbations are common in electrical circuits and can cause consequences in beam operation on measurements with the ADT.

The 50 Hz harmonic has been observed in the LHC transverse beam spectrum since the start of operation [61, 62], arising from a power supply ripple. The harmonics are visible throughout the transverse beam spectrum, rather than around the driven tune. The sidebands from a transverse beam excitation with the ADT have not been observed before.

Additional frequency lines were observed around the main ADT tune line Q_x^{ADT} aside from the secondary spectral lines. Sidebands were observed in measurements with different working points both at injection energy and at top energy. As the excitation amplitude of the ADT at top energy is low, the amplitude of the sidebands is not sufficient in both beams and planes to be observed above the noise floor and thus the sidebands are discussed in this chapter at injection energy. With the ac dipole the sidebands were not present in the frequency spectrum as seen in previous figures in this chapter, and it can be concluded that the sidebands indeed originate from a 50 Hz modulation of the ADT waveform.

Figure 5.42 shows the frequency spectra of the horizontal and vertical planes of Beam 1 for an ADT measurement during MD9549 zoomed in around the ADT tune. Three sidebands are observed in the horizontal and vertical frequency spectra, with first order sidebands at frequencies $Q_{u,d} \pm Q_{50\mathrm{Hz}}$, where $Q_{u,d}$ is the driven tune with $u \in \{x, y\}$ and $Q_{50\mathrm{Hz}} = \frac{50\ \mathrm{Hz}}{11245\ \mathrm{Hz}} \approx 4.45 \times 10^{-3}$. The frequency $11245\ \mathrm{Hz}$ is the revolution frequency of the LHC, describing the number of turns the particles make per second. In addition, a second order sideband is observed in the horizontal spectrum at the frequency of $Q_{x,d} + 2Q_{50\mathrm{Hz}}$ and in the vertical spectrum at frequency of $Q_{y,d} - 2Q_{50\mathrm{Hz}}$. The amplitude response of the sidebands is asymmetric, and increases when their frequency is approaching the natural tune. From this it can be determined that the three sidebands can be treated as three weaker separate ac dipoles, each causing a kick to the beam. Correspondingly similar figures can be created to ADT measurements at injection during recommissioning, as well as high-β^* measurements.

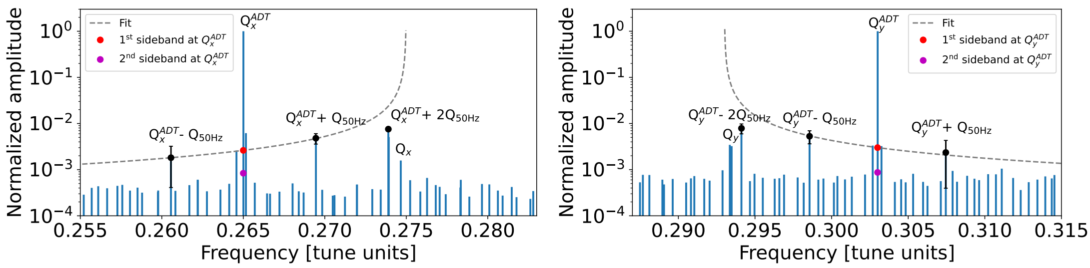

Figure 5.42. *Frequency spectrum of horizontal (left) and vertical (right) planes of Beam 1 at injection energy during MD9549, zoomed in around the main mode. The relative strengths of the first and second order 50 Hz sidebands at the frequency of the driven tune Q_x^{ADT} are shown in red and magenta.*

The betatronic amplitude response of an ac dipole follows the relation

$$A_p = \frac{\sqrt{\beta_{\mathrm{ADT}}}\hat{B}_p/(4B_0\rho)}{\sin\left(\pi(Q_{u,d} + p \cdot Q_{50\mathrm{Hz}}) - Q_u\right)}, \tag{5.1}$$

where the numerator denotes the effective strength of an ac dipole associated to the p^{th} sideband, where β_{ADT} is the β-function at the location of the ADT, $\hat{B}_p$ is the integrated magnetic field and $B_0\rho$ is the magnetic rigidity [42]. As the strength of the sideband increases when approaching the natural tune, the tune split with opposite signs for each plane results in a symmetric distribution of the visible tune lines. With Eq. 5.1, the relative strength of the sidebands with respect to the main excitation at the frequency of the driven tune can be determined.

The average amplitude of the sidebands was calculated over all BPMs. For the first order sidebands, the average strengths were fit to the measured data using Eq. 5.1 and the relative strength at the ADT tune frequency was determined by interpolating the fit in that specific frequency. Since only one of the second order sidebands is visible in the frequency spectrum, applying a fit based on a single point would not have been sensible, but the relative strength could still be determined with only one second order sideband. The relative strength from the visible second order sideband at the ADT frequency was determined with Eq. 5.1. The relative strengths for first and second sidebands for measurements at injection during MD9549 and during recommissioning of ADT acquisition are shown in Table 5.2. The strengths were calculated for three measurements through all BPMs and averaged.

Table 5.2. *Measured relative strengths of the 50 Hz sidebands* $(B_1/B_0$ *and* $B_2/B_0)$ *for both beams and both planes at injection energy.*

		First sideband [10^{-3}]	**Second sideband [10^{-3}]**
MD9549	B1 H	2.64 ± 0.10	0.85 ± 0.03
	B1 V	3.02 ± 0.05	0.90 ± 0.03
	B2 H	2.19 ± 0.12	0.58 ± 0.02
	B2 V	2.72 ± 0.08	0.42 ± 0.03
Recommissioning	B1 H	2.61 ± 0.15	0.86 ± 0.04
	B1 V	2.78 ± 0.09	0.59 ± 0.04
	B2 H	2.15 ± 0.04	1.52 ± 0.06
	B2 V	2.69 ± 0.12	0.51 ± 0.01

The relative strengths of the sidebands at the ADT frequency have some variation by beam and plane. For the first order sideband, the relative strength is between $(2.15 - 3.02) \times 10^{-3}$, and the variation between beam and plane agrees with both measurement sets, with the highest relative strength measured with the horizontal plane of Beam 1. The variation by beam and plane match to the measured actions in Table 5.1 with a lower oscillation amplitude corresponding to a higher relative strength of the sideband.

For the second order sideband, the relative strength varies between $(0.42-1.52)\times 10^{-3}$, with no correlation between the measured actions. Some discrepancy can be observed for the horizontal plane of Beam 2 during recommissioning measurements, where the second sideband strength is notably larger than for Beam 1. The horizontal natural tune had varied during measurements, and the tune for Beam 2 was lower than with Beam 1 at around $Q_{x,\mathrm{B2}} = 0.2794$. Since the second order sideband is very close to the natural tune, the sideband is amplified and the relative strength is larger. If the change in the tune is adapted in calculations, the relative strength of the second order sideband for the horizontal plane of Beam 2 during recommissioning is $(0.74 \pm 0.03) \times 10^{-3}$. This observation highlights the sensitivity of measurements with the ADT.

The strength of the sidebands is larger than expected, but simulation studies showed that the 50 Hz modulation does not have an effect on ADT performance in terms of beam stability for collective effects [63]. Further studies are needed to fully determine whether the presence of the sidebands contributes to emittance growth.

Since the sidebands can be treated as individual ac dipoles each providing a kick to the beam, optics parameters using the first order sideband tune as the driven tune were calculated. Naturally the sidebands would not be used for measuring optics since their amplitudes are much lower than the amplitude of the ADT tune, and the analysis was performed out of pure curiosity. Optics functions were calculated to sidebands of ADT measurements during MD9549, and the β-beating with the sidebands optics is shown in Figs. 5.43 and 5.44 for Beam 1 and Beam 2, respectively. As expected, the oscillation amplitude of the sideband is lower than with the driven tune, resulting in peak β-beating of over 50 %.

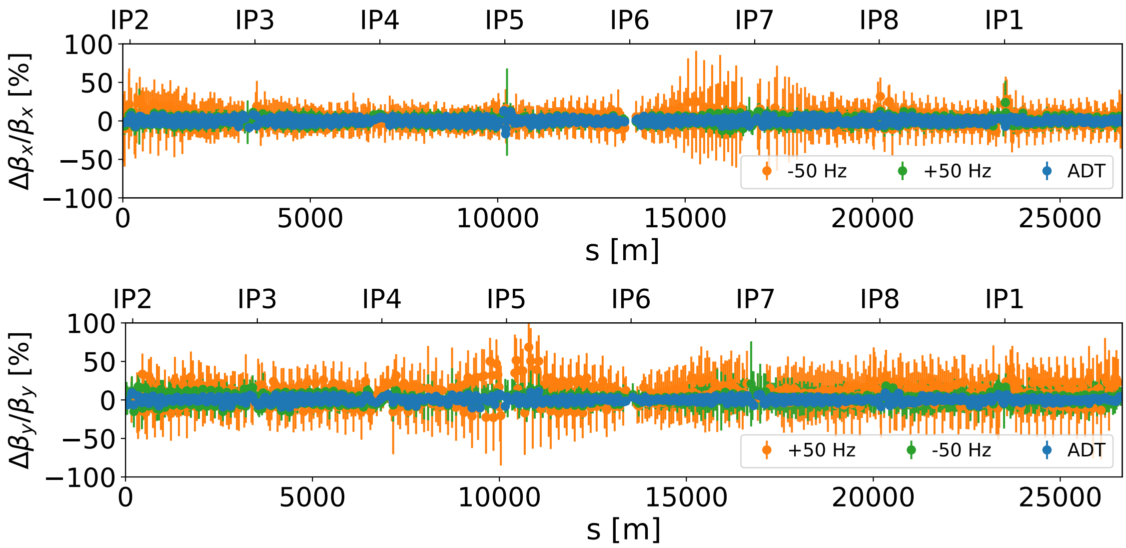

Figure 5.43. *Horizontal (top) and vertical (bottom) β-beating of Beam 1 at injection using the sidebands as driven tunes. ADT indicates the actual driven tune used, and -50 Hz and +50 Hz indicate the sideband tune used.*

The total phase difference between the main driven ADT tune and the first order sidebands was calculated, and it is shown in Figs. 5.45 and 5.46 for Beam 1 and Beam 2, respectively. The total phase difference was calculated for three individual measurements separately.

As expected, the observed phase difference is symmetrical between the first order sidebands. The source is still unclear on what is causing this behaviour, and in the future the effect of possible amplitude, phase, or frequency modulation should be looked into. In addition, the offset of the phase difference seems random, making the noise not synchronised with the ADT.

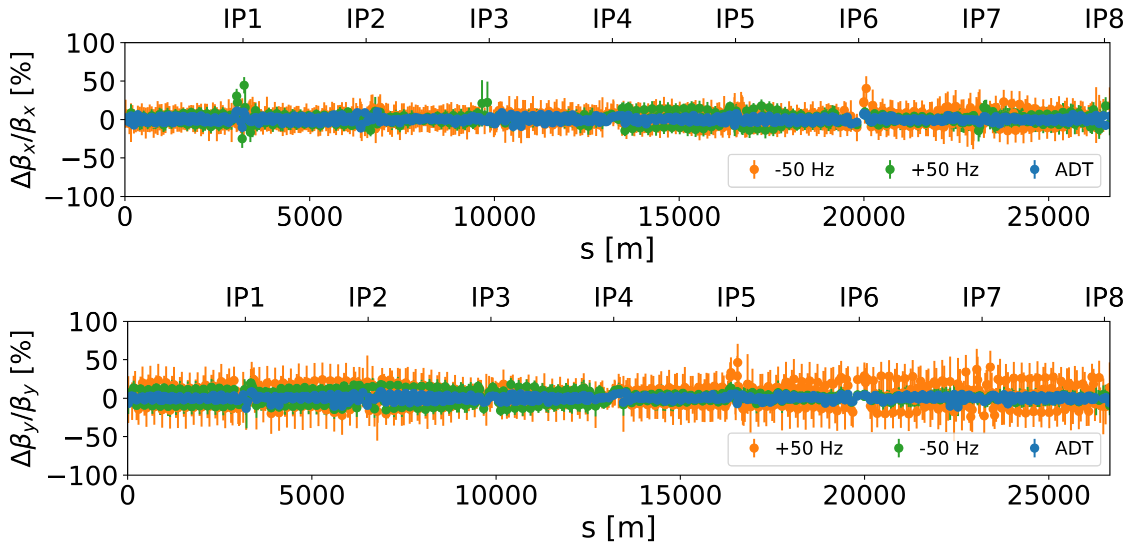

Figure 5.44. *Horizontal (top) and vertical (bottom) β-beating of Beam 2 at injection using the sidebands as driven tunes. ADT indicates the actual driven tune used, and -50 Hz and +50 Hz indicate the sideband tune used.*

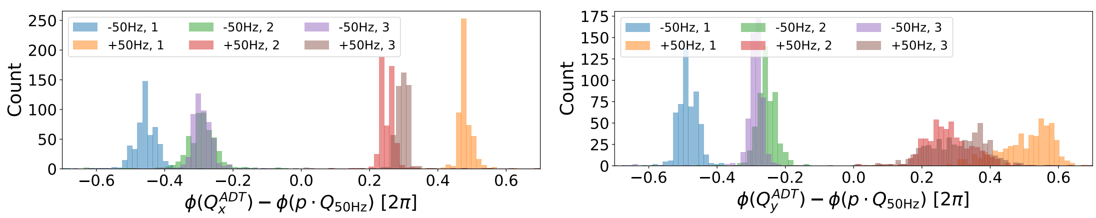

Figure 5.45. *Horizontal (left) and vertical (right) total phase difference between the driven tune and first order sidebands of Beam 1 for three individual measurements.*

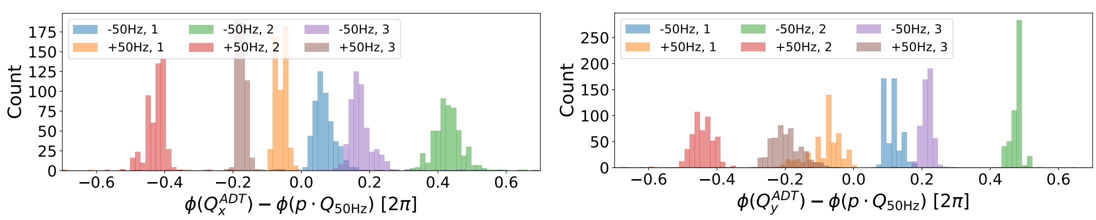

Figure 5.46. *Horizontal (left) and vertical (right) total phase difference between the driven tune and first order sidebands of Beam 2 for three individual measurements.*

6. CONCLUSION

This thesis presents developments towards reliable and reproducible optics measurements using the ADT. Current optics measurements in the LHC are performed using an ac dipole, which is limited to low-intensity non-colliding bunches. In order to gather information about optics during operation, using the ADT in ac dipole -like mode for transverse beam excitations is considered. This offers a safe option in operational conditions due to the weaker strength of the ADT.

An important reduction of the noise floor of the frequency spectrum was achieved by making three changes to the measurement conditions of ADT excitations. The excitation amplitude was set to the current maximum setting, and further increased by reducing the tune split, specifically in the vertical plane. In addition, the number of acquired turns was increased from 6600 to 40 000, improving the spectral resolution even further to equivalent level with ac dipole measurements for linear optics. The signal-to-noise ratio of the achieved maximum ADT beam excitation improved by a factor of 8, agreeing with high-amplitude ac dipole measurements.

ADT measurements at injection energy showed good agreement with reference ac dipole measurements on two different working points. Although the oscillation amplitude of ADT excitations is lower than with the ac dipole, the β-beating agrees with both working points within the errors of ac dipole measurements. The results prove that the ADT can reliably be used for linear optics measurements in the LHC.

To validate the quality of optics measurements with the ADT at top energy, ADT beam excitations were performed at 6.8 TeV during two different commissioning campaigns. Optics were successfully measured with the ADT with $\beta^*_{\mathrm{IP1,IP5}} = 30\ \mathrm{cm}$ and $\beta^*_{\mathrm{IP1,IP5}} = 120\ \mathrm{m}$, although the oscillation amplitude limited the quality of the measurements. A higher oscillation amplitude would improve the spectral resolution, which would result in a better agreement with the ac dipole.

Results of this thesis showed that ADT optics measurements can be used to identify possible deviations in the optics. Measurements during the ramp of the ion cycle showed a decrease in optics quality at around 6.3 TeV. Similar behaviour of the optics was observed with ADT and ac dipole beam excitations, even with 6600 turns of ADT excitations.

In addition to the linear optics measurements, first observations of resonance driving terms at injection with the ADT were analysed. Normal sextupolar RDTs $f_{0111,V}$ and $f_{1020,V}$ showed an excellent agreement between the ADT and the ac dipole with measurements performed during recommissioning. Some variance between the two excitation methods was observed with the $f_{1200,H}$ and $f_{3000,H}$ RDTs, possibly due to the lower oscillation amplitude of the ADT. The investigations offer an interesting possibility for measuring resonance driving terms with low-amplitude ADT beam excitations in the future. Nonlinear beam dynamics studies with the ADT could be performed by exciting the beam closer to the resonance.

One method to measure machine nonlinearities is to measure amplitude detuning. This was attempted as a part of ADT measurements performed in 2023 by varying the oscillation amplitude during the measurement. Although notable amplitude detuning was not observed with the ADT, decreasing the tune split would increase the oscillation amplitude, thus increasing the sensitivity to amplitude detuning. The current software for ADT acquisitions only permits diagonal kicks, i.e. having the same set oscillation amplitude for the horizontal and vertical plane. An upgrade on the current software with more variability on setting the oscillation amplitude by plane would allow for measuring amplitude detuning in a single transverse variable with the ADT.

Additionally, 50 Hz sidebands were observed in the frequency spectra of ADT measurements at injection. The relative strength of the first and second order sidebands at the frequency of the ADT tune was $(2.60 \pm 0.09) \times 10^{-3}$ and $(0.78 \pm 0.03) \times 10^{-3}$, respectively, and the strengths were larger than expected. Further studies are needed to mitigate the phenomenon and study the possible effects of the sidebands for emittance growth and collective effects.

Improvements to ADT excitations performed in this thesis open up a wide range of research for low-amplitude optics measurements. Validation of linear optics with the ADT gives the possibility to measure optics at the start of each fill in the LHC, giving information about possible optics deviations during the operational year. This procedure would require new software for automatic analysis of the optics since experts are not always available.

ADT measurements at top energy still require further validation to correspond to the precision with ac dipole excitations. A smaller tune split would increase the oscillation amplitude, benefitting the spectral resolution. As the ADT is considered safe to use in operational conditions with high-intensity bunches and bunch trains, measurements with these conditions would give even more information on optics during operation. Measurements with bunches with nominal intensity would be a reasonable next step in the project.

REFERENCES

[1] I. Béjar Alonso, O. Brüning, P. Fessia, M. Lamont, L. Rossi, L. Tavian and M. Zerlauth, eds. High-Luminosity Large Hadron Collider (HL-LHC): Technical design report. CERN Yellow Reports: Monographs. CERN, 2020. DOI: 10.23731/CYRM-2020-0010.

[2] K. Paraschou, H. Bartosik, L. Deniau, G. Iadarola, E. H. Maclean, L. Mether, Y. Papaphilippou, T. Pieloni, J. M. B. Potdevin, G. Rumolo and R. Tomás García. Emittance Growth From Electron Clouds Forming in the LHC Arc Quadrupoles. *Proc. 68th Adv. Beam Dyn. Workshop High-Intensity High-Brightness Hadron Beams (HB'23)* (Geneva, Switzerland). JACoW Publishing, Geneva, Switzerland, Apr. 2024, pp. 487–490. DOI: 10.18429/JACoW-HB2023-THBP16.

[3] R. Tomás, F. Carlier, F. Chudoba, L. Deniau, J. Dilly, V. Ferrentino, S. Horney, M. Hostettler, J. Keintzel, S. Kostoglou, M. Le Garrec, E. H. Maclean, T. Nissinen, K. Paraschou, T. Persson, M. Solfaroli, F. Soubelet, A. Wegscheider and J. Wenninger. Optics for Landau damping with minimized octupolar resonances in the LHC. *Journal of Instrumentation* 19 (May 2024), T05010. DOI: 10.1088/1748-0221/19/05/T05010.

[4] L. E. Medina Medrano, J. Barranco García, X. Buffat, T. Pieloni and R. Tomás. Assessment of Linear and Non-Linear Optics Errors due to Beam-Beam with Multipoles for the High Luminosity LHC. *Proc. 9th International Particle Accelerator Conference (IPAC'18)* (Vancouver, BC, Canada). JACoW Publishing, Geneva, Switzerland, June 2018, pp. 3557–3560. DOI: 10.18429/JACoW-IPAC2018-THPAK135.

[5] P. Gonçalves Jorge, J. Barranco, T. Pieloni, X. Buffat, F. S. Carlier, J. Coello de Portugal, E. Fol, L. Medina, R. Tomás and A. Wegscheider. Measurement of Beta-Beating due to Strong Head-on Beam-Beam Interactions in the LHC. *Proc. 8th International Particle Accelerator Conference (IPAC'17)* (Copenhagen, Denmark). JACoW Publishing, Geneva, Switzerland, May 2017, pp. 2121–2124. DOI: 10.18429/JACoW-IPAC2017-TUPVA030.

[6] T. Persson, X. Buffat, J. Dilly, M. Hostettler, E. H. Maclean, U. Kar, K. Skoufaris, G. Sterbini and R. Tomás. MD12263 - Weak-Strong investigation of Long-Range Beam-beam. Presented at the LHC Studies Working Group meeting. July 2, 2024. URL: https://indico.cern.ch/event/1430777/.

[7] T. Persson, F. Carlier, J. Coello de Portugal, A. Garcia-Tabares Valdivieso, A. Langner, E. H. Maclean, L. Malina, P. Skowronski, B. Salvant, R. Tomás and A. C. García Bonilla. LHC optics commissioning: A journey towards 1% optics control. *Phys.*

Rev. Accel. Beams 20 (June 2017), p. 061002. DOI: 10.1103/PhysRevAccelBeams.20.061002.

[8] E. H. Maclean, R. Tomás, F. S. Carlier, M. S. Camillocci, J. W. Dilly, J. Coello de Portugal, E. Fol, K. Fuchsberger, A. Garcia-Tabares Valdivieso, M. Giovannozzi, M. Hofer, L. Malina, T. H. B. Persson, P. K. Skowronski and A. Wegscheider. New approach to LHC optics commissioning for the nonlinear era. *Phys. Rev. Accel. Beams* 22 (June 2019), p. 061004. DOI: 10.1103/PhysRevAccelBeams.22.061004.

[9] R. Tomás, T. Bach, R. Calaga, A. Langner, Y. I. Levinsen, E. H. Maclean, T. H. B. Persson, P. K. Skowronski, M. Strzelczyk, G. Vanbavinckhove and R. Miyamoto. Record low β beating in the LHC. *Phys. Rev. ST Accel. Beams* 15 (Sept. 2012), p. 091001. DOI: 10.1103/PhysRevSTAB.15.091001.

[10] T. Persson, A. Börjesson Carazo, F. Carlier, F. Chudoba, J. Dilly, R. De Maria, S. Fartoukh, V. Ferrentino, E. Fol, S. Horney, U. Kar, J. Keintzel, M. Le Garrec, E. H. Maclean, T. Nissinen, F. Soubelet, K. Skoufaris, G. Trad, R. Tomás, L. Van Riesen-Haupt, W. Van Goethem, A. Wegscheider and J. Cardona. LHC optics commissioning in 2023 and 2024. *Proc. 15th International Particle Accelerator Conference (IPAC'24)* (Nashville, TN). JACoW Publishing, Geneva, Switzerland, May 2024, pp. 67–70. DOI: 10.18429/JACoW-IPAC2024-MOPC12.

[11] F. S. Carlier. A Nonlinear Future - Measurements and corrections of nonlinear beam dynamics using forced transverse oscillations. PhD thesis. University of Amsterdam, 2020. URL: https://cds.cern.ch/record/2715765.

[12] J. Dilly. Corrections of high-order nonlinearities in the LHC and High-Luminosity LHC beam optics. PhD thesis. Humboldt-Universität zu Berlin, 2024. URL: https://cds.cern.ch/record/2895574.

[13] M. Söderén, J. Komppula, G. Kotzian, S. Rains and D. Valuch. ADT and Obsbox in LHC Run 2, Plans for LS2. *Proc. of the 9th Evian Workshop on LHC Beam Operations* (Evian, France). CERN, Geneva, Switzerland, Feb. 2019, pp. 165–171. URL: https://cds.cern.ch/record/2750292.

[14] O. S. Brüning, P. Collier, P. Lebrun, S. Myers, R. Ostojic, J. Poole and P. Proudlock. LHC Design Report. Vol. 1: The LHC Main Ring. CERN Yellow Reports: Monographs. CERN, 2004. DOI: 10.5170/CERN-2004-003-V-1.

[15] The ATLAS Collaboration. The ATLAS Experiment at the CERN Large Hadron Collider. *JINST* 3 (2008), S08003. DOI: 10.1088/1748-0221/3/08/S08003.

[16] The CMS Collaboration. The CMS Experiment at the CERN LHC. *JINST* 3 (2008), S08004. DOI: 10.1088/1748-0221/3/08/S08004.

[17] The LHCb Collaboration. The LHCb Detector at the LHC. *JINST* 3 (2008), S08005. DOI: 10.1088/1748-0221/3/08/S08005.

[18] The ALICE Collaboration. The ALICE Experiment at the CERN LHC. *JINST* 3 (2008), S08002. DOI: 10.1088/1748-0221/3/08/S08002.

[19] The ATLAS Collaboration. Observation of a new particle in the search for the Standard Model Higgs boson with the ATLAS detector at the LHC. *Physics Letters B* 716 (Sept. 2012), pp. 1–29. DOI: 10.1016/j.physletb.2012.08.020.

[20] The CMS Collaboration. Observation of a new boson at a mass of 125 GeV with the CMS experiment at the LHC. *Physics Letters B* 716 (Sept. 2012), pp. 30–61. DOI: 10.1016/j.physletb.2012.08.021.

[21] P. Langacker. The Standard Model and Beyond. 2nd ed. CRC Press, 2017. DOI: 10.1201/b22175.

[22] M. Vretenar, ed. Linac4 design report. Vol. 6. CERN Yellow Reports: Monographs. CERN, 2020. DOI: 10.23731/CYRM-2020-006.

[23] The Proton Synchrotron Booster. Accessed on 15.6.2024. URL: https://home.cern/science/accelerators/proton-synchrotron-booster.

[24] The Proton Synchrotron. Accessed on 15.6.2024. URL: https://home.cern/science/accelerators/proton-synchrotron.

[25] The Super Proton Synchrotron. Accessed on 15.6.2024. URL: https://home.cern/science/accelerators/super-proton-synchrotron.

[26] Linear accelerator 3. Accessed on 15.6.2024. URL: https://home.cern/science/accelerators/linear-accelerator-3.

[27] The Low Energy Ion Ring. Accessed on 15.6.2024. URL: https://home.cern/science/accelerators/low-energy-ion-ring.

[28] E. Lopienska. The CERN accelerator complex, layout in 2022. General Photo. 2022. URL: https://cds.cern.ch/record/2800984.

[29] J. Wenninger. Machine Protection and Operation for LHC. *Proceedings of the 2014 Joint International Accelerator School: Beam Loss and Accelerator Protection*. Vol. 2. CERN, Geneva, Switzerland, 2016. DOI: 10.5170/CERN-2016-002.377.

[30] R. Alemany Fernández. LHC commissioning plans. Sept. 2007. URL: https://indico.cern.ch/event/24517.

[31] S. Y. Lee. Accelerator Physics (Fourth Edition). World Scientific Publishing Company, 2018.

[32] H. Wiedemann. Particle accelerator physics. Springer Nature, 2015.

[33] A. Wolski. Beam Dynamics in High Energy Particle Accelerators. Imperial College Press, 2014.

[34] Proceedings of the CERN Accelerator School course: Introduction to Particle Accelerators. URL: https://cas.web.cern.ch/previous-schools.

[35] E. Courant and H. Snyder. Theory of the alternating-gradient synchrotron. *Annals of Physics* 3 (1958), pp. 1–48. DOI: 10.1016/0003-4916(58)90012-5.

[36] A. Franchi. Studies and measurements of linear coupling and nonlinearities in hadron circular accelerators. PhD thesis. Johann Wolfgang Goethe-Universität, 2006. URL: https://d-nb.info/981264875/34.

[37] F. Soubelet. fsoubelet/PyhDToolkit. 2024. DOI: 10.5281/zenodo.4268804.

[38] L. R. Carver, X. Buffat, K. Li, E. Métral and M. Schenk. Transverse beam instabilities in the presence of linear coupling in the Large Hadron Collider. *Phys. Rev. Accel. Beams* 21 (Apr. 2018), p. 044401. DOI: 10.1103/PhysRevAccelBeams.21.044401.

[39] S. White, E. Maclean and R. Tomás. Direct amplitude detuning measurement with ac dipole. *Phys. Rev. ST Accel. Beams* 16 (July 2013), p. 071002. DOI: 10.1103/PhysRevSTAB.16.071002.

[40] J. Dilly, V. Ferrentino, M. Le Garrec, E. H. Maclean, L. Malina, T. Persson, T. Pugnat, L. van Riesen-Haupt, F. Soubelet and R. Tomás. First operational dodecapole correction in the LHC. *Phys. Rev. Accel. Beams* 26 (12 Dec. 2023), p. 121001. DOI: 10.1103/PhysRevAccelBeams.26.121001.

[41] J. Serrano and M. Cattin. *The LHC AC Dipole system: an introduction*. Tech. rep. CERN, 2010. URL: https://cds.cern.ch/record/1263248.

[42] R. Tomás. Normal form of particle motion under the influence of an ac dipole. *Phys. Rev. ST Accel. Beams* 5 (May 2002), p. 054001. DOI: 10.1103/PhysRevSTAB.5.054001.

[43] F. S. Carlier, R. Tomás, E. H. Maclean and T. H. B. Persson. First experimental demonstration of forced dynamic aperture measurements with LHC ac dipoles. *Phys. Rev. Accel. Beams* 22 (Mar. 2019), p. 031002. DOI: 10.1103/PhysRevAccelBeams.22.031002.

[44] R. Tomás. Adiabaticity of the ramping process of an ac dipole. *Phys. Rev. ST Accel. Beams* 8 (Feb. 2005), p. 024401. DOI: 10.1103/PhysRevSTAB.8.024401.

[45] D. Valuch, W. Höfle, G. Kotzian, M. Jaussi, S. Rains, M. Ojeda-Sandonís and M. Söderén. ADT and OBSBOX in 2016. *Proc. of the 7th Evian Workshop on LHC Beam Operations* (Evian, France). CERN, Geneva, Switzerland, Dec. 2016, pp. 181–184. URL: https://cds.cern.ch/record/2293530.

[46] G.-H. Hemelsoet, A. Calia, K. Fuchsberger, M. Gabriel, M. Hostettler, M. Hruska, D. Jacquet, T. Persson, M. Soderen and D. Valuch. Online Coupling Measurement and Correction Throughout the LHC Cycle. *Proc. of 16th International Conference on Accelerator and Large Experimental Control Systems (ICALEPCS'17)* (Barcelona, Spain). JACoW Publishing, Geneva, Switzerland, Jan. 2018, pp. 686–691. DOI: 10.18429/JACoW-ICALEPCS2017-TUPHA119.

[47] M. Wendt. BPM Systems: A brief Introduction to Beam Position Monitoring. *Proceedings of the CERN Accelerator School course on Beam Instrumentation, Tuusula, Finland*. 2018, pp. 355–393. DOI: 10.48550/arXiv.2005.14081.

[48] Optics Measurements and Corrections -team. URL: https://pylhc.github.io.

[49] L. Malina. Harpy: A Fast, Simple and Accurate Harmonic Analysis with Error Propagation. *Proc. 13th International Particle Accelerator Conference (IPAC'22)* (Bangkok, Thailand). JACoW Publishing, Geneva, Switzerland, July 2022, pp. 2326–2329. DOI: 10.18429/JACoW-IPAC2022-WEPOMS035.

[50] P. Castro. Luminosity and beta function measurement at the electron-positron collider ring LEP. PhD thesis. University of Valencia, 1996. URL: https://cds.cern.ch/record/316609.

[51] L. Deniau, H. Grote, G. Roy and F. Schmidt. The MAD-X Program - User's Reference Manual. URL: http://cern.ch/madx/releases/last-rel/madxuguide.pdf.

[52] A. Langner and R. Tomás. Optics measurement algorithms and error analysis for the proton energy frontier. *Phys. Rev. ST Accel. Beams* 18 (Mar. 2015), p. 031002. DOI: 10.1103/PhysRevSTAB.18.031002.

[53] A. Wegscheider, A. Langner, R. Tomás and A. Franchi. Analytical N beam position monitor method. *Phys. Rev. Accel. Beams* 20 (Nov. 2017), p. 111002. DOI: 10.1103/PhysRevAccelBeams.20.111002.

[54] O. S. Brüning and S. D. Fartoukh. *Field Quality Specification for the LHC Main Dipole Magnets*. Tech. rep. Geneva: CERN, 2001. URL: https://cds.cern.ch/record/522049.

[55] M. Le Garrec, J. Dilly, V. Ferrentino, S. Horney, E. H. Maclean and T. Nissinen. MD9549 – Non-Linear Optics at Injection. (2024). To be published.

[56] The LHC leak repair: a short photostory. URL: https://home.cern/news/news/accelerators/lhc-leak-repair-short-photostory.

[57] TOTEM Experiment. Accessed on 24.10.2023. URL: https://home.cern/science/experiments/totem.

[58] ALFA - Absolute Luminosity for ATLAS. Accessed on 24.10.2023. URL: https://atlas-project-lumi-fphys.web.cern.ch/ALFA/.

[59] R. Bruce. Losses in the ion energy ramp. Presented at the LNO-NDC joint meeting. Nov. 3, 2023. URL: https://indico.cern.ch/event/1342836.

[60] T. Persson. Optics measurements in the ion energy ramp. Presented at the LNO-NDC joint meeting. Nov. 3, 2023. URL: https://indico.cern.ch/event/1342836.

[61] S. Kostoglou, G. Arduini, Y. Papaphilippou, G. Sterbini and L. Intelisano. Origin of the 50 Hz harmonics in the transverse beam spectrum of the Large Hadron Collider. *Phys. Rev. Accel. Beams* 24 (Mar. 2021), p. 034001. DOI: 10.1103/PhysRevAccelBeams.24.034001.

[62] S. Kostoglou, H. Bartosik, G. Sterbini and M. Söderén. Harmonics of 50 Hz on the beam spectrum of the Large Hadron Collider. *Proc. 14th International Particle Accelerator Conference* (Venice, Italy). JACoW Publishing, Geneva, Switzerland, May 2023, pp. 606–609. DOI: 10.18429/JACoW-IPAC2023-MOPL035.

[63] X. Buffat. Are the ADT 50 Hz sidebands a concern (for the beam stability)? Presented at the 225th HiLumi WP2 Meeting. Jan. 12, 2024. URL: https://indico.cern.ch/event/1359556.

APPENDIX A: HB PROCEEDINGS: LHC OPTICS MEASUREMENTS FROM TRANSVERSE DAMPER FOR THE HIGH INTENSITY FRONTIER

This appendix presents the proceedings paper submitted for the 68th ICFA Advanced Beam Dynamics Workshop on High-Intensity and High-Brightness Hadron Beams (HB2023) that was organized at CERN in Geneva, Switzerland. The paper presents ADT measurement results at injection energy, summarising linear and nonlinear optics results taken during MD9549.

68th Adv. Beam Dyn. Workshop High-Intensity High-Brightness Hadron Beams HB2023, Geneva, Switzerland JACoW Publishing
ISBN: 978-3-95450-253-0 ISSN: 2673-5571 doi:10.18429/JACoW-HB2023-THBP14

LHC OPTICS MEASUREMENTS FROM TRANSVERSE DAMPER FOR THE HIGH INTENSITY FRONTIER

T. Nissinen*, F. Carlier, M. Le Garrec, E. H. Maclean, T. H. B. Persson, R. Tomás, A. Wegscheider, CERN, Geneva, Switzerland

Abstract

Current and future accelerator projects are pushing the brightness and intensity frontier, creating new challenges for turn-by-turn based optics measurements. Transverse oscillations are limited in amplitude due to particle losses. The LHC Transverse Damper (ADT) is capable of generating low amplitude ac-dipole like transverse coherent beam oscillations. While the amplitude of such excitations is low, it is compensated by the excitation length of the ADT which, in theory, can last for up to 48h. Using the ADT, it is possible to use the maximum BPM acquisition length and improve the spectral resolution. First optics measurements have been performed using the ADT in the Large Hadron Collider in 2023, and the results are presented in this paper. Furthermore, some observed limitations of this method are presented and their impact on ADT studies are discussed.

INTRODUCTION

Optics measurements from transverse turn-by-turn data are generally carried out with a single low intensity bunch to limit particle losses from the ac-dipole forced betatron oscillations [1]. This is particularly important for high energy accelerators where machine protection constraints are tight. Under such conditions the effects of high bunch intensities and large number of bunches on the optics are not measured. As bunch intensities are pushed further, the resulting optics perturbations become more relevant. Optics measurements under these conditions can yield valuable insights and provide new paths for machine optimisation.

Optics measurements in the Large Hadron Collider (LHC) are mostly performed by exciting coherent transverse oscillations using an ac-dipole [2–8]. These oscillations are measured at Beam Position Monitors (BPMs) around the ring. The spectral analysis of such signals provides amplitude and phase information of the main modes of oscillation from which the optics functions are calculated, as described in Refs. [9–11]. In the LHC, the ac dipole generates large amplitude, 6600 turns flattop excitations. In this paper, the ADT is used in an ac dipole-like mode, as an alternative excitation method to provide low amplitude coherent oscillation with a duration close the maximum recording limit of the BPMs. While lower in amplitude, the increase in number of turns provides an important improvement in the spectral resolution. Most importantly, the ac dipole may not be used with more than 3 low intensity bunches, while the ADT is considered safe for using during nominal operational conditions. It should be mentioned that in operation large chromaticity and Landau octupoles are used to mitigate coherent instabilities.

* tnissine@cern.ch

These have an impact in the optics measurement technique that requires further studies [5, 6, 8, 11]. The ADT therefore opens up the possibility to perform optics measurements at the LHC intensity limit.

This paper describes the progress in performing linear and non-linear optics measurements using the LHC ADT in ac dipole mode. The first optics measurements are presented at injection energy with pilot bunches. Lastly, an analysis of the observed sidebands on the ADT excitation resulting from 50 Hz noise is presented.

PHASE RESOLUTION FROM TURN-BY-TURN DATA

The phase error on the main betatronic oscillation has been calculated from the spectral analysis of single BPM turn-by-turn data for different excitation conditions. Figure 1 shows the phase error obtained from turn-by-turn data of ac dipole and ADT excitations as a function of oscillation amplitude. A clear reduction of phase errors is observed for increasing oscillation amplitudes. Figure 1 also shows the measured betatron spectral phase error for ADT excitations with larger number of turns considering a single excitation per point. The phase resolution from ADT driven oscillations matches that from the ac dipole at injection energy.

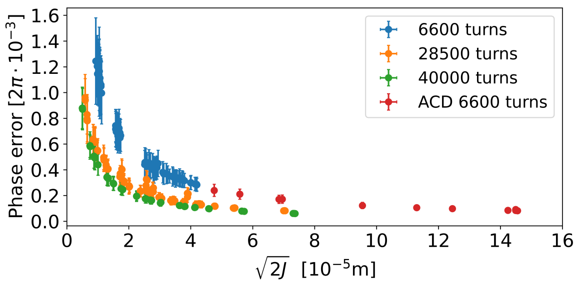

Figure 1: Phase error from ADT and ac dipole (ACD) excitations as a function of oscillation amplitude for different number of turns.

OPTICS MEASUREMENTS WITH THE ADT

Since the end of Run 2 the ADT is used for calculating coupling corrections during the nominal physics cycle in the LHC [12], and they are part of the operational procedure at the start of each fill. The aim of the current studies is to demonstrate the feasibility of performing optics measurements using the ADT, with the future goal of integrating this feature in the operational tools. Optics measurements were performed using the ADT with pilot bunches at injection

Content from this work may be used under the terms of the CC BY 3.0 licence (© 2021). Any distribution of this work must maintain attribution to the author(s), title of the work, publisher, and DOI

68th Adv. Beam Dyn. Workshop High-Intensity High-Brightness Hadron Beams HB2023, Geneva, Switzerland JACoW Publishing
ISBN: 978-3-95450-253-0 ISSN: 2673-5571 doi:10.18429/JACoW-HB2023-THBP14

Content from this work may be used under the terms of the CC BY 3.0 licence (© 2021). Any distribution of this work must maintain attribution to the author(s), title of the work, publisher, and DOI

energy with 28500 turns of coherent oscillations. These measurements were obtained during a dedicated Machine Development (MD). Figure 2 shows the measured β-beating for Beam 1 for a section of the machine, compared to the reference ac dipole measurements. A good agreement is observed between the ADT and ac dipole measurements, and is representative for both beams and both planes. Figure 3 shows the difference between the β-beating observed from the two methods compared to the errors from the ac dipole measurements. The observed deviation is generally within the measurement errors of the ac dipole measurements, thus demonstrating that optics measurements can reliably be done with the ADT at injection energy. The operational procedure could therefore be adapted by increasing the number of acquired turns for ADT measurements at the start of each fill to perform routine optics measurements at injection.

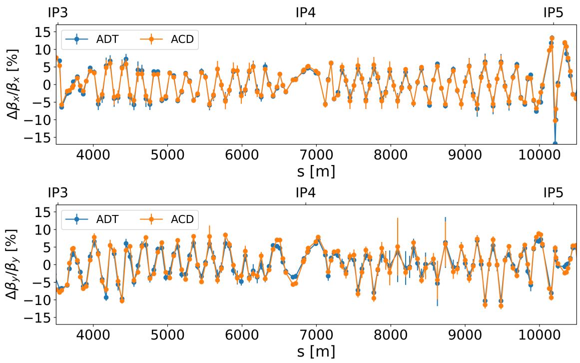

Figure 2: Comparison of horizontal and vertical β-beating of Beam 1 between ADT and ac dipole measurements. The data shown is a representative sample of the whole machine for both beams.

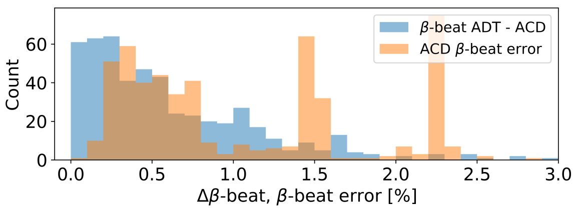

Figure 3: Comparison of difference in β-beating between the ADT and ac dipole measurements and β-beating error for the ac dipole for the horizontal plane of Beam 1.

RESONANCE DRIVING TERMS WITH LOW AMPLITUDE EXCITATIONS

The improved spectral resolution due to the increased number of turns may be of further benefit for measuring resonance driving terms (RDTs) [13–16] using low amplitude excitations. This could allow the measurements of nonlinear optics while reducing the risks of beam losses. If validated for nominal beam intensities this could provide valuable linear and nonlinear optics measurements for machine conditions that are currently restricted, such as with bunch trains.

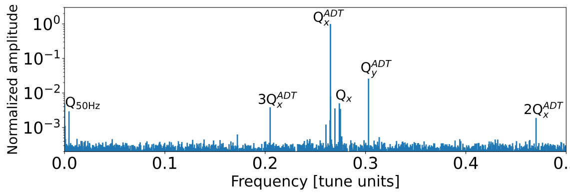

Figure 4: Frequency spectrum of the horizontal plane for Beam 2. Secondary spectral lines are observed at the frequencies $2Q_x^{ADT}$ (normal sextupole) and $3Q_x^{ADT}$ (normal octupole).

Figure 4 shows the spectrum obtained from horizontal turn-by-turn data from an ADT excitation at injection energy in Beam 2. Aside from the main ADT lines, two secondary spectral lines arising from nonlinear sources are clearly observed at frequencies $2Q_x^{ADT}$ and $3Q_x^{ADT}$. Furthermore, several sidebands are observed around the main ADT mode, and will be discussed in the following section.

The line at frequency $2Q_x^{ADT}$ is related to the normal sextupolar RDTs f_{1200} and f_{3000}, while the line at frequency $3Q_x^{ADT}$ is related to the normal octupolar RDTs f_{1300} and f_{4000}. From these measurements, the corresponding driving terms can be calculated. Figure 5 shows the calculated normal sextupolar driving terms f_{1200} and f_{3000} measured with ADT and ac dipole excitations. While the RDT amplitude variations are lost in ADT measurements, possibly due to their small excitation amplitudes, some qualitative agreement is observed between both methods. The results are promising and motivate further studies to improve sextupolar RDT measurements with the ADT.

The normal octupolar RDTs f_{1300} and f_{4000} show a large discrepancy between the ADT and the ac dipole, which could originate from a saturation of the ADT signal. Further investigations are required.

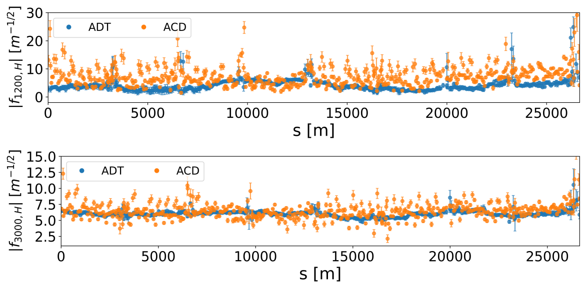

Figure 5: Comparison of normal sextupolar RDTs f_{1200} (top) and f_{3000} (bottom) for Beam 2 between ADT and ac dipole measurements.

OBSERVATION OF 50 Hz SIDEBANDS IN THE ADT

50 Hz sidebands were observed in the frequency spectra around the ADT tune, both at injection energy and at top

ISBN: 978-3-95450-253-0 ISSN: 2673-5571 doi:10.18429/JACoW-HB2023-THBP14

Table 1: Measured relative strengths of the 50 Hz sidebands (B_1/B_0 and B_2/B_0) for both beams and both planes.

	1st sideband [10^{-3}]	2nd sideband [10^{-3}]
B1 H	2.64 ± 0.10	0.85 ± 0.03
B1 V	3.02 ± 0.05	0.90 ± 0.03
B2 H	1.98 ± 0.11	0.57 ± 0.02
B2 V	2.62 ± 0.08	0.41 ± 0.03

energy. An example frequency spectrum for the horizontal plane of Beam 1 at injection energy, zoomed in around the main mode, is shown in Fig. 6. The spectra exhibit three clear sidebands at frequencies $Q_{x,d} \pm Q_{50Hz}$ and $Q_{x,d} + 2Q_{50Hz}$, with $Q_{50Hz} = 4.45 \times 10^{-3}$. The sidebands are most likely generated by a 50 Hz modulation of the ADT waveform, and function as three weaker ac dipoles on the beam motion. Indeed, the amplitude response of the sidebands is asymmetric and increases as their frequency approaches the natural tune. The spectrum shown in Fig. 6 is representative of all BPMs and for both beams.

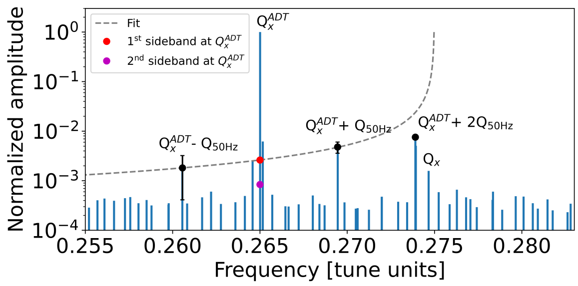

Figure 6: Strength of the 50 Hz sidebands at the frequency of the driven ADT tune.

The relative strength of the sidebands with respect to the ADT kick strength can be estimated by treating the sidebands as ac dipoles. The betatronic amplitude response follows the following relation [5],

$$A_p = \frac{B_p}{\sin\left(\pi(Q_{x,d} + p \cdot Q_{50Hz}) - Q_x\right)}, \quad (1)$$

where $B_p = \sqrt{\beta_{ADT}}\hat{B}_p/(4B_0\rho)$ represents the effective strength of an ac-dipole associated to the p^{th} sideband, $p \in$ {-1, 1, 2}. β_{ADT} is the β function at the ADT, $\hat{B}_p$ is the integrated magnetic field and $B_0\rho$ is the magnetic rigidity. Using this equation, the relative strength of the sideband can be determined. The average amplitude of the sidebands is calculated over all BPMs. Using these averaged amplitudes, the sideband strengths are fit to the measured data using Eq. (1) for the two first order sidebands to interpolate their amplitude at the location of the ADT tune, as shown in Fig. 6. The measured relative strengths of the 50 Hz sidebands are shown in Table 1.

The strength of the 50 Hz sidebands are larger than previously expected, and their presence in the transverse damper may be a source of emittance growth during operational use

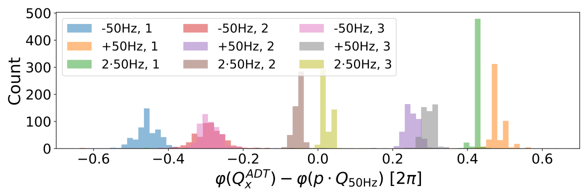

Figure 7: Horizontal phase difference for Beam 1 between ADT and sidebands for three measurements.

of the ADT. Further studies on the effect of such sidebands on operational use are currently ongoing.

Figure 7 shows the phase difference between the main spectral line from the ADT and its sidebands. For the first order sidebands with $p = \pm 1$, the phase difference is of opposite sign. Further analysis is required to fully characterize the the ADT modulation.

CONCLUSIONS

The LHC Transverse Damper (ADT) is considered safe for use in operational conditions. It thus allows for exciting ac dipole-like coherent transverse oscillations at high beam intensities in the LHC, and opens the door for optics measurements at machine conditions that were previously restricted.

Coherent transverse oscillations are successfully excited using the ADT in ac dipole mode, for a duration beyond the BPM limits. Such excitations are lower in amplitude than the LHC ac dipole, but increase the number of acquired turns from 6600 to 40000 turns, yielding similar phase error than the AC dipole at injection energy.

Optics measurements performed using the ADT at injection energy with pilot bunches show a good agreement with reference measurements performed with the ac dipole. Increasing the number of turns to 40000 in the ADT excitations for coupling corrections in operational procedures could yield fill-by-fill optics measurements at injection.

First explorations of the measurements of normal sextupolar and octupolar RDTs with ADT excitations show promising results requiring further developments.

Lastly, significant 50 Hz sidebands are observed around the main ADT tune line in the spectra of turn-by-turn data. This indicates a 50 Hz modulation of the ADT waveform, with a strength of (0.25±0.04)% and (0.069±0.02)% in the first and second order sidebands, respectively. The phase of the first order sidebands with $p = \pm 1$ have opposite signs, as expected, for example, from amplitude modulation. Further studies are needed to fully characterize the ADT unwanted modulation and estimate its potential detrimental effects.

ACKNOWLEDGEMENTS

The authors would like to thank the LHC Operations team for the support during the measurements campaigns in the LHC.

Content from this work may be used under the terms of the CC BY 3.0 licence (© 2021). Any distribution of this work must maintain attribution to the author(s), title of the work, publisher, and DOI

ISBN: 978-3-95450-253-0 ISSN: 2673-5571 doi:10.18429/JACoW-HB2023-THBP14

Content from this work may be used under the terms of the CC BY 3.0 licence (© 2021). Any distribution of this work must maintain attribution to the author(s), title of the work, publisher, and DOI

REFERENCES

[1] F. S. Carlier, R. Tomás, E. H. Maclean, and T. H. B. Persson, "First experimental demonstration of forced dynamic aperture measurements with LHC ac dipoles", *Phys. Rev. Accel. Beams*, vol. 22, p. 031002, 2019. doi:10.1103/PhysRevAccelBeams.22.031002

[2] R. Tomás *et al.*, "CERN Large Hadron Collider optics model, measurements, and corrections", *Phys. Rev. Spec. Top. Accel Beams*, vol. 13, p. 121004, 2010. doi:10.1103/PhysRevSTAB.13.121004

[3] R. Tomás *et al.*, "Record low β-beating in the LHC", *Phys. Rev. Spec. Top. Accel. Beams*, vol. 15, p. 091001, 2012. doi:10.1103/PhysRevSTAB.15.091001

[4] T. Persson *et al.*, "LHC injection optics commissioning in 2021 and 2022", Rep. CERN-ACC-NOTE-2023-0015, 2023.

[5] R. Tomás, "Normal form of particle motion under the influence of an ac dipole", *Phys. Rev. Spec. Top. Accel. Beams*, vol. 5, p. 054001, 2002. doi:10.1103/PhysRevSTAB.5.054001

[6] R. Tomás, "Adiabaticity of the ramping process of an ac dipole", *Phys. Rev. Spec. Top. Accel. Beams*, vol. 8, p. 024401, 2005. doi:10.1103/PhysRevSTAB.8.024401

[7] R. Tomás, "Direct Measurement of Resonance Driving Terms in the Super Proton Synchrotron (SPS) of CERN using Beam Position Monitors", Ph.D. thesis, University of Valencia, Spain, 2003, Rep. CERN-THESIS-2003-010.

[8] F. S. Carlier, "A Nonlinear Future - Measurements and corrections of nonlinear beam dynamics using forced transverse oscillations", Ph.D. thesis, University of Amsterdam, The Netherlands, 2020, Rep. CERN-THESIS-2020-025.

[9] A. Wegscheider, A. Langner, R. Tomás, and A. Franchi, "Analytical N beam position monitor method", *Phys. Rev. Accel. Beams*, vol. 20, p. 111002, 2017. doi:10.1103/PhysRevAccelBeams.20.111002

[10] A. García-Tabares and R. Tomás, "Optics-measurement-based beam position monitor calibrations in the LHC insertion regions", *Phys. Rev. Accel. Beams*, vol. 23, p. 042801, 2020. doi:10.1103/PhysRevAccelBeams.23.042801

[11] L. Malina, R. Tomás, H. Timko, D. Louro Alves, and J. Coello de Portugal, "LHC MD 4505: Forced 3D beam oscillations", Rep. CERN-ACC-NOTE-2020-0065, 2020.

[12] G. H. Hemelsoet *et al.*, "Online Coupling Measurement and Correction Throughout the LHC Cycle", in *Proc. ICALEPCS'17*, Barcelona, Spain, Oct. 2017, pp. 686–691. doi:10.18429/JACoW-ICALEPCS2017-TUPHA119

[13] M. Benedikt, F. Schmidt, R. Tomás, P. Urschütz, and A. Faus-Golfe, "Driving Term Experiments at CERN", *Phys. Rev. Spec. Top. Accel. Beams*, vol. 10, p. 034002, 2007. doi:10.1103/PhysRevSTAB.10.034002

[14] A. Franchi, R. Tomás, and F. Schmidt, "Magnet strength measurement in circular accelerators from beam position monitor data", *Phys. Rev. Spec. Top. Accel. Beams*, vol. 10, p. 074001, 2007. doi:10.1103/PhysRevSTAB.10.074001

[15] R. Tomás, M. Bai, R. Calaga, W. Fischer, A. Franchi, and G. Rumolo, "Measurement of global and local resonance terms", *Phys. Rev. Spec. Top. Accel. Beams*, vol. 8, p. 024001, 2005. doi:10.1103/PhysRevSTAB.8.024001

[16] A. Wegscheider and R. Tomás Garcia, "Forced Coupling Resonance Driving Terms", in *Proc. IPAC'21*, Campinas, Brazil, May 2021, pp. 3646–3649. doi:10.18429/JACoW-IPAC2021-WEPAB400